High-Order Embedded Finite Difference Schemes for Initial Boundary Value Problems on Time Dependent Irregular Domains. *

Adi Ditkowski †, Yuval Harness †

November 11, 2007

Abstract

This paper considers a family of spatially discrete approximations, including boundary treatment, to initial boundary value problems in evolving bounded domains. The presented method is based on the Cartesian grid embedded Finite-Difference method, which was initially introduced by Abarbanel and Ditkowski [24] [25], for initial boundary value problems on constant irregular domains.

We perform a comprehensive theoretical analysis of the numerical issues, which arise when dealing with domains, whose boundaries evolve smoothly in the spatial domain as a function of time. In this class of problems the moving boundaries are impenetrable with either Dirichlet or Neumann boundary conditions, and should not be confused with the class of moving interface problems such as multiple phase flow, solidification, and the stefan problem.

Unlike other similar works on this class of problems, the resulting method is not restricted to domains of up to 3-D, can achieve higher then 2^{nd}-order accuracy both in time and space, and is strictly stable in semi-discrete settings. The strict stability property of the method also implies that the numerical solution remains consistent and valid for a long integration time.

A complete convergence analysis is carried in semi-discrete settings, including a detailed analysis for the implementation of the diffusion equation. Numerical solutions of the diffusion equation, using the method for a 2^{nd} and a 4^{th}-order of accuracy are carried out in one dimension and two dimensions respectively, which demonstrates the efficacy of the method.

*This research was supported by the ISRAEL SCIENCE FOUNDATION (grant No. 1362/04).

†School of Mathematical Sciences, Tel Aviv University, Tel Aviv 69978, Israel

1 Introduction

This paper considers numerical solutions of initial boundary value problems (**IBVPs**), on domains with time moving boundaries. Such problems occur in many science and engineering problems, and can generally be divided into two types:

Moving Interface Problems: The physical domain is divided into several non-overlapping connected sub-domains, each representing distinct material (such as water and oil) or state (such as water and ice). The parameters in the governing differential equations are typically discontinuous across the interfaces separating the distinct sub-domains. Usually the interfaces are only known at some initial time point, and must be determined as part of the solution as it evolves with time. Multiple phase flow, and Hele-Shaw cells for pattern formation are some of the better known examples [1] [2] [3].

Moving Impenetrable Boundary Problems: The physical domain is either subject to time evolving deformation, and/or contains moving solids whose interior is not governed by a differential equation. Typically the moving boundary is considered impenetrable with either Dirichlet or Neumann boundary conditions, and it's movement is either given or known explicitly from the solution. Flow with moving solid bodies, and heat transfer in arbitrary moving geometries, are typical examples [2] [3].

For both types of problems the shape of the boundary/interface can be complex, and can undergo change, merge, and breakup during the course of the simulation. Consequently it is both difficult and computationally expensive to use body-fitted grid methods, which require an adaptive processes of grid generation and adjustment to the evolving boundary/interface. A fixed cartesian grid, where the boundary/interface can cut through the grid line is often used, this approach greatly reduces the complexity of the computation, and can be implemented much more easily.

The class of methods, which employ a fixed cartesian grid with the boundary/interface embedded into the scheme are termed Embedded Methods. The most popular methods used are, among others, the immersed

boundary method (IBM) originally developed by Peskin [5] for simulating blood flow in the heart (see review by Peskin [6]), the ghost fluid method (GF) of Fedkiw et al. [7][8][9], and the immersed interface method (IIM), which was initially introduced by LeVeque and Li [11] for elliptic interface problems [12]. A similar idea to the IIM was used earlier by Mayo [10].

When using a fixed cartesian grid, one inevitably has to deal with grid crossing events, which occurs when the boundary/interface passes over some grid-point. This phenomena implies different numerical considerations for each type of problem: In the case of Moving Interface Problems, this means that grid points are shifting from one side of the interface to the opposite side, but remain at all time within the computational domain. In the case of Moving Impenetrable Boundary Problems, this means that grid points are entering or exiting the computational domain, which usually requires an extrapolation procedure to initialize values that are uncovered as the boundary moves.

Though this paper considers only Moving Impenetrable Boundary Problems, it should be mentioned that for Moving Interface Problems the requirement to determine the location of the interfaces using a fixed cartesian grid employs a boundary capture technique, which attempts to follow the boundary motion against a fixed computational grid. An important method used for the boundary capturing is the Level-Set method [14] [15]. Both The IBM and the IIM have been incorporated in the level-set method (for example see [13]).

Concerning Moving Impenetrable Boundary Problems the IIM and other sharp interface methods have been developed for flow with moving solid bodies [16][17][18][19][20]. For the heat equation on irregular time dependent domains, Colella et al. [21][22], presented a solution algorithm using a Finite-Volume approach. However, all these methods attained up to 2^{nd}-order accuracy, were validated for geometrically simple domains of up to 3-D, and without a rigorous proof of convergence.

In this work we present a method based on the Cartesian grid embedded Finite-Difference method, which was initially introduced by Abarbanel and Ditkowski [24] [25], for initial boundary value problems on constant irregular

domains. We perform a comprehensive theoretical analysis of the numerical issues, that arise when dealing with time dependent domains, including treatment of mergers, and breakups of the moving boundary, which may occur during the course of the simulation. A complete convergence analysis is given in semi-discrete settings, and the resulting method is shown to be strictly stable and applicable to irregular time dependent domains of arbitrary finite dimension. We impose few restrictions as possible on the boundary movement. This paper summarizes the results presented in "Embedded Finite-Difference Schemes for Initial Boundary Value Problems in Time Dependent Complex Domains" [4].

The subsequent sections are organized as follows:
In section 2, we present the framework for constructing finite-difference approximations using Cartesian grids on moving-boundary geometries. In section 3, we deal with the geometric aspects of approximating functions on Cartesian grids in complex moving geometries. In section 4, we analyze the convergence of semi-discrete approximations, which maintain the order of accuracy with a strict stability. In section 5, we establish the notations and assumptions for applying the method. In section 6, we apply the method for the diffusion equation, with Dirichlet boundary conditions. Numerical examples of 2^{nd}-order and 4^{th}-order accurate schemes are presented in section 7.

2 General Theory and Concepts

In this section a general theory and concepts of applying the **Embedded Finite-Difference** Method for IBVPs with moving boundaries, are presented.

2.1 Problem Formulation

2.1.1 IBVP with Moving Boundaries

Let us consider the problem,

$$\frac{\partial u}{\partial t} = L(u) + f(\boldsymbol{x}, t), \tag{2.1}$$

$$u(\boldsymbol{x}, 0) = u_0(\boldsymbol{x}), \tag{2.2}$$

$$B(u(\boldsymbol{x}, t))\,|_{\partial\Omega(t)} = u_B(t), \tag{2.3}$$

where B and L are linear differential operators. The problem is assumed to be well posed, and defined for all $\boldsymbol{x} \in \Omega(t) \subset \mathbb{R}^{\mathrm{d}}$ and all $t \geq 0$, where $\Omega(t)$ is a time-dependent domain.

2.1.2 Domain and Boundary Curve Properties

For the multi-dimensional case we assume:

- The boundary is a smooth curve, given by a known function,

$$\partial\Omega(t) = \left\{ \boldsymbol{\Gamma}(t) \in C\left(\mathbb{R}^d\right) \right\}, \quad \boldsymbol{\Gamma}(t) \in \mathbb{R}^d, \quad \forall\, t \geq 0, \tag{2.4}$$

  which satisfies

$$|\partial_n \boldsymbol{\Gamma}| \leq c \quad \textit{and} \quad R_\Gamma(t) > R_{min} \quad \forall\, t \geq 0, \tag{2.5}$$

  where $R_\Gamma(t)$ denotes the *Radius of Curvature* at $\boldsymbol{\Gamma}(t) \in \partial\Omega(t)$.
  This requirement assures that using a fine enough grid, the set of internal grid-points, which are valid for the numerical approximation is maximized. Furthermore, this set of valid internal grid points, always maintains a certain bounded proximity to the boundary (see section **2.2.1** for details).

- The domain is a connected bounded set in $\mathbb{R}^d$ for all $t \geq 0$.

2.2 A Brief Introduction to Embedded Finite-Difference

The particular approach we use was originally developed by Abarbanel and Ditkowski [24] [25], which generalized [23]. The method has been applied successfully to IBVPs on constant domains by embedding the boundary operator into the numerical scheme in a penalty-based approach, see for example [26], [27], [28], [29].

2.2.1 The One-Dimensional Model

Consider a one-dimensional problem, with Dirichlet boundary conditions,

$$\frac{\partial u}{\partial t} = L(u) + f(x,t), \tag{2.6}$$

$$u(x,0) = u_0(x), \tag{2.7}$$

$$u(\Gamma_{L/R},t) = g_{L/R}(t), \tag{2.8}$$

Let us spatially discretize (2.6) on the following uniform grid:

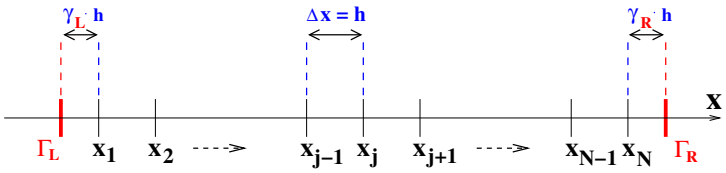

Figure 2.1: One Dimensional Spatial Discretization

where the internal grid points are set by $x_{j+1} - x_j = h$ for $1 \le j \le N$, with respect to the boundary points:

$$x_1 - \Gamma_L = \gamma_L h,\ \Gamma_R - x_N = \gamma_L h$$

such that $0 \le \gamma_L, \gamma_R \le 1$. Note that, the boundary points, Γ_L and Γ_R, do not necessarily coincide with the the extremal grid-points, x_1 and x_N.
The projection of the exact solution onto the grid is $u_j(t) := u(x_j,t)$ and similarly $f_j(t) := f(x_j,t)$ is the projection of the inhomogeneous term. Let L_N be a matrix approximating the differential operator, L, at internal grid-points, then the semi-discrete form of (2.6) becomes:

$$\frac{d\boldsymbol{U}}{dt} = (L_N\boldsymbol{U} + \boldsymbol{T.E.}) + (B_N\boldsymbol{U} + \boldsymbol{E.E.}) + \boldsymbol{F}(t), \tag{2.9}$$

where $\boldsymbol{U}$ and $\boldsymbol{F}$ are gridfunction vectors of the exact solution and the inhomogeneous term respectively:

$$\boldsymbol{U} := (u_1, u_2 ... u_N)^T, \quad \boldsymbol{F} := (f_1, f_2 ... f_N)^T$$

$\boldsymbol{T.E.}$ is the truncation error of the numerical approximation at internal grid points, B_N is a numerical boundary operator, and $\boldsymbol{E.E.}$ is the extrapolation error of B_N near the boundary. Accordingly, we set the boundary operator by

$$B_N \boldsymbol{U} = -T_L \left(A_L \boldsymbol{U} - \boldsymbol{G}_L \right) - T_R \left(A_R \boldsymbol{U} - \boldsymbol{G}_R \right), \tag{2.10}$$

where $\boldsymbol{G}_{L/R} := (1, 1, \dots 1)^T g_{L/R}$ are boundary value vectors, $T_{L/R}$ are diagonal weights matrices, and $A_{L/R}$ are extrapolations to the boundary matrices satisfying the relation

$$A_{L/R} \boldsymbol{U} = \boldsymbol{G}_{L/R} + \boldsymbol{E.E}_{L/R}, \tag{2.11}$$

i.e, each row in $A_{L/R}$ is an extrapolation functional, which extrapolates $B(u)$, and the extrapolation error is then given by $\boldsymbol{E.E}_{L/R}$.
By omitting the truncation error, $\boldsymbol{T.E.}$, and the extrapolation error, $\boldsymbol{E.E.}$, we get the following semi-discrete scheme:

$$\frac{d\boldsymbol{V}}{dt} = M\boldsymbol{V} + \overline{\boldsymbol{G}} + \boldsymbol{F}, \tag{2.12}$$

where $\boldsymbol{V}$ is the gridfunction of the approximate solution, $M := L_N - T_L A_L - T_R A_R$, and $\overline{\boldsymbol{G}} := T_L \boldsymbol{G}_L + T_R \boldsymbol{G}_R$. Accordingly, we seek weights matrices, T_L and T_R, for which the matrix M is Negative-Definite (**N.D**) for a parabolic operator and Non-Positive-Definite (**N.P.D**) for a hyperbolic operator, which implies strict-stability of the scheme (2.12).

2.2.2 The Multi-Dimensional Model

For a general multi-dimensional problem, whose differential operator does not have mixed derivatives, $L = \sum_{r=1}^{d} L^{(x_r)}$, we may set a separate numerical operator in each coordinate direction.
Indeed, when the matrix representation in each coordinate direction is N.D (N.P.D) then the overall scheme is represented by an N.D (N.P.D) matrix, since the sum of two N.Ds (N.P.Ds) is N.D (N.P.D). This is the sense in which such schemes are 'modular'.

2.2.3 The Error Boundness Property

Denoting $\boldsymbol{E} := \boldsymbol{U} - \boldsymbol{V}$ and subtracting (2.12) from (2.9), we have

$$\frac{d}{dt}\left|\boldsymbol{E}\right| \leq -\bar{c}\left|\boldsymbol{E}\right| + \left|\boldsymbol{T}\right|, \quad \left|\boldsymbol{E}\right| = \left\langle \boldsymbol{E}, \boldsymbol{E}\right\rangle^{1/2}, \tag{2.13}$$

where $\langle \cdot, \cdot \rangle$ denotes the standard scalar product, $\boldsymbol{T}$ denotes the total of the extrapolation and truncation errors, and

$$\bar{c} := -\max\left\{\sigma\left(M^S\right)\right\}, \quad M^S := \left(M + M^T\right)/2, \tag{2.14}$$

where $\sigma\left(T\right)$ denotes the *spectrum of the operator* T.
Accordingly, by Gronwall's lemma, we have

$$\left|\boldsymbol{E}\right| \;\leq\; \left\|\boldsymbol{T}\right\|_\infty \begin{cases} h^m \frac{1-e^{-\bar{c}t}}{\bar{c}} & \text{if } M \text{ is } \textbf{N.D.} \\ h^m t & \text{if } M \text{ is } \textbf{N.P.D.} \end{cases} \tag{2.15}$$

$$\left\|\boldsymbol{T}\right\|_\infty := \max_{0\leq s\leq t} \left|\boldsymbol{T}(s)\right| / h^m, \tag{2.16}$$

where h is the spatial mesh size and m is the spatial order of accuracy.

2.3 The Embedded Finite-Difference for Moving Boundaries

The major difficulty in applying the Embedded Finite-Difference Method for IBVP with Moving Boundaries accounts for the uniform fixed grid employed by the algorithm. Indeed, as the boundary evolves with time, we need to deal with events of grid-points entering or exiting the domain, which greatly complicates the analysis and implementation of the scheme.

2.3.1 The Algorithm

In practice, the approximation $\boldsymbol{V}$ is obtained by applying some multi-stage or multi-step method with (2.12), where stability is assured under conditions given in Kreiss and Wu [30] or Levy and Tadmor [31].
For simplicity, we assume $\boldsymbol{V}$ is evaluated at constant time steps,

$$t_0 := 0\ ,\ t_n := n \cdot k \quad \forall n \in \mathbb{N}, \tag{2.17}$$

and opt to apply the following algorithm at every temporal sub-interval, $T_n := (t_n, t_{n+1})$:

1. **Suspension:** tag as *suspended* any grid-point which enters or exits the domain at some $t^* \in T_n$.

2. **Numerical solution:** apply a numerical solution over $\boldsymbol{V}_I(t_n)$, the vector of the approximate gridfunction solution at t_n, on internal and not *suspended* grid-points, and obtain $\boldsymbol{V}_I(t_{n+1})$.

3. **Extrapolation for the next temporal subinterval:** insert the approximate solution at the newly entered grid-points at t_{n+1}, via polynomial extrapolation for T_{n+1}.

3 Geometric Consideration

In this section the geometric considerations for applying the Embedded Finite-Difference Method in a time-dependent domain, are discussed. We distinguish between a **genuine one-dimensional** domain, and a **one-dimensional section** of a multi-dimensional domain.

3.1 The One Dimensional Model

3.1.1 Domain Properties

Now, at a given time point $t \geq 0$, we expect, the following representation of the domain:

$$\Omega(t) := \{x \in \Omega^{(q)}(t) \mid q = 1, 2 \dots q_f\} \; = \; \bigcup_{q=1}^{q_f} \Omega^{(q)}(t), \quad \Omega^{(q)}(t) := (\Gamma_L^{(q)}, \Gamma_R^{(q)}), \tag{3.1}$$

where $\left\{\Omega^{(q)}(t)\right\}$ are spatial non-overlapping open intervals, whose boundary points, $\left\{\Gamma_{L/R}^{(q)}\right\}$, evolve smoothly with t. The boundary's evolution in time inserts and extracts grid-points into and from the domain, which are tagged as *suspended* within each temporal sub-interval, T_n.

Moreover, since we opt to use the one-dimensional model as a building block for multi-dimensional problems, we expect $\boldsymbol{q}_f$, the number of open intervals, to vary in time, due to the following events:

- **Sub-Domains Merger:** at some time point, t^*, two boundary points belonging to sequential sub-domains join together, thus the two sub-domains merge to one-sub-domain, as displayed in Figure 3.1.

- **Sub-Domain Split:** at some time point, t^*, a new boundary is emerging in the interior of the domain, thus a sub-domain is split into two sub-domains, as displayed in Figure 3.1.

- **Sub-Domain Depletion:** at some time point, t^*, two boundary points of the same sub-domain join together and from that point on, the sub-domain is depleted and removed from the domain, as displayed in Figure 3.2.

- **Sub-Domain Emergence:** at some time point, a new boundary is emerging outside the domain, and a new sub-domain is emerging, as displayed in Figure 3.2.

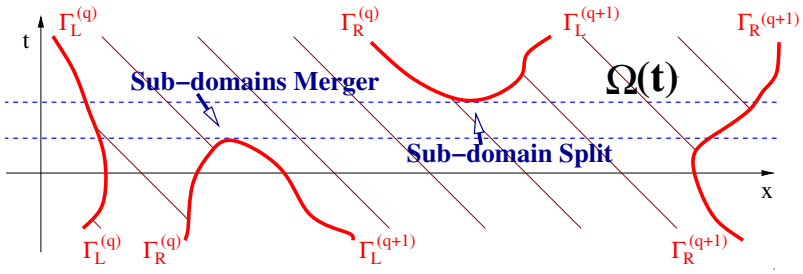

Figure 3.1: Permissible Events

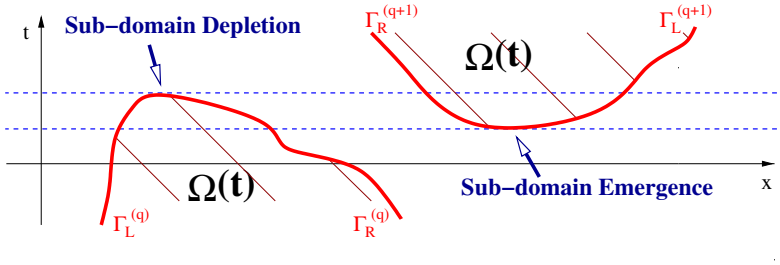

Figure 3.2: Impermissible Events

If the given problem is genuinely one-dimensional, i.e. the domain is purely one-dimensional,

- **Merger/Split** events may insert/extract into/from the domain grid-points, which reside spatially far from the boundary.

- **Depletion/Emergence** events lead inevitably to scarcity of grid-points in the sub-domain, which implies degraded accuracy and non-existence of a **CFL** condition. Hence, are considered impermissible.

If the problem is multi-dimensional, i.e. the one-dimensional domain is a one-dimensional section of a multi-dimensional domain:

- **Merger/Split** events insert/extract into/from the domain grid-points, with spatial proximity to the boundary in at least one coordinate direction.

- **Depletion/Emergence** events need not be considered impermissible, if the *Radius of Curvature* has a uniform lower bound. See sub-section 3.2.1 for details.

3.1.2 Boundary Movement

The algorithm suggested in section 2.3.1 is applicable assuming the boundary's position moves slowly with respect to $\Delta x/\Delta t = h/k$. Accordingly, for a genuine one-dimensional problem, we require

$$\max_{t\in[t_n,t_{n+1}]}\left|\frac{d}{dt}\Gamma^{(q)}_{L/R}(t)\right| < \frac{h}{2k} \quad \Rightarrow \quad \sup_{t\in T_n}\left|\Gamma^{(q)}_{L/R}(t) - \Gamma^{(q)}_{L/R}(t_n)\right| < \frac{h}{2}, \tag{3.2}$$

Hence, at each T_n,

$$\inf\left\{|\partial\Omega(t) - x_j| \mid x_j \in X_I(t)\right\} \leq 3h/2, \tag{3.3}$$

where $X_I(t)$ denotes the set of internal and not *suspended* grid-points at $t \in T_n$. Note that, (3.2) is the maximal lower bound, for which a Merger/Split event may insert/extract into/from the domain, at most one grid-point, as displayed in Figure 3.3.

3.2 The Multi-Dimensional Model

Let $\mathcal{S} := 2s+1$ be the number of grid-points required by the scheme's stencil in any coordinate direction, x_r, for some $s \in \mathbb{N}$. Accordingly,

- We say that a sequence of internal grid-points in any coordinate direction, containing more than $2s$ grid-points, is an $\mathcal{S}$-*line*.

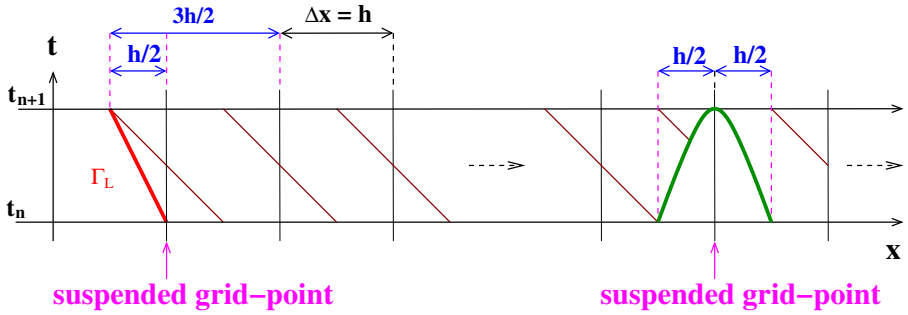

Figure 3.3: One-Dimensional Boundary Movement

- We say an internal grid-point, $\boldsymbol{x}_j$, intersected only by $\mathcal{S}$-*lines*, is an *admissible* grid-point.

3.2.1 Domain Properties

We minimize the set of internal non-*admissible* grid-points, by applying the following requirements:

1. **Intersection condition:** An $\mathcal{S}$-*line* may intersect a non-$\mathcal{S}$-*line*, only at the $\mathcal{S}$-*line*'s extreme grid-points. Hence, narrow slots with respect to mesh size ,as displayed in Figure 3.4, are prohibited.

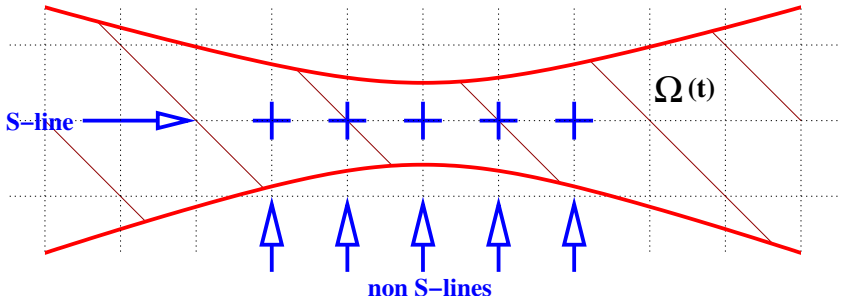

Figure 3.4: Narrow Slot Example

2. **Curvature condition:** at any boundary point, $\boldsymbol{\Gamma}(t)$, the *Radius of Curvature*, $R_\Gamma(t)$, must satisfy

$$R_\Gamma(t) > R_{min} := h\left(1/4 + s^2\right). \tag{3.4}$$

Hence, as displayed in Figure 3.5,

$$\inf \{|\partial\Omega(t) - \boldsymbol{x}_j| \mid \boldsymbol{x}_j \in X_A(t)\} \leq 3h/2, \tag{3.5}$$

where $X_A(t)$ denotes the set of *admissible* grid-points at $t \geq 0$.

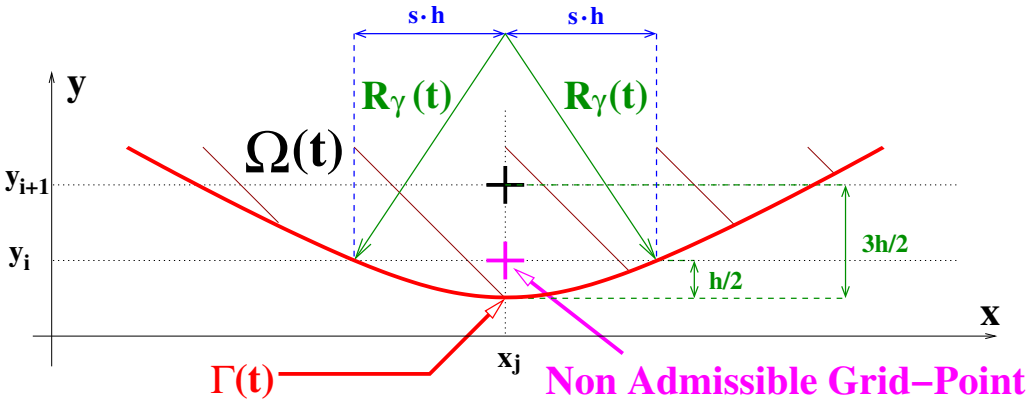

Figure 3.5: *Radius of Curvature* Example

Though this property is preserved over $X_I(t_n)$, for all n, it may not be preserved over $X_I(t)$, for all $t \in T_n$, due to the multi-dimensional nature of the boundary's movement.

3.2.2 Boundary Movement

Analogously to the one-dimensional case, we require the following bound over the normal derivative of the boundary:

$$\forall n \quad \max_{t\in[t_n,t_{n+1}]} |\nabla_n \partial\Omega(t)| < \frac{h}{2k}, \tag{3.6}$$

However, this requirement does not ensure that the boundary's movement of any one-dimensional section of the domain satisfies the requirement of the genuine one-dimensional case. For example consider the boundary movement of the two dimensional domain as displayed in Figure 3.6.

Although the normal derivative of the boundary's movement is bounded, the one dimensional y-section of the domain at $\boldsymbol{y}_1$ exhibits a much faster movement, which does not satisfy requirement (3.2).

Such extreme cases may occur when the boundary has a very large (or infinite) radius of curvature with a front parallel to one of the axes. Hence,

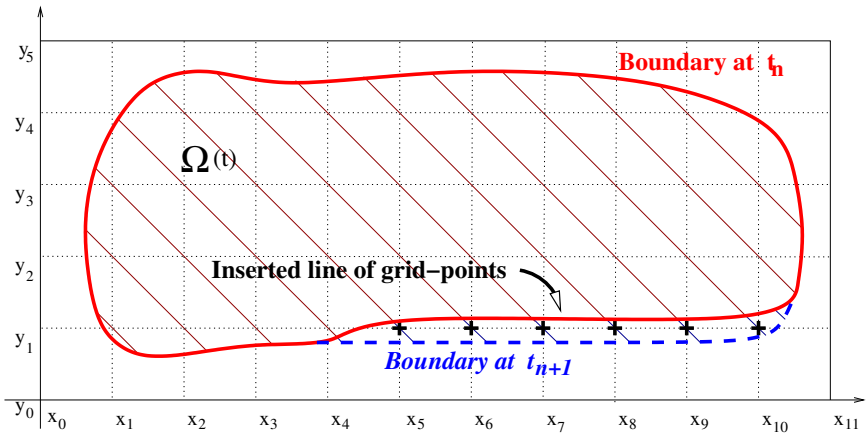

Figure 3.6: Multi-Dimensional Boundary Movement

unlike the genuine one-dimensional case, we may encounter an almost unbounded boundary velocity of any one-dimensional section of the domain, due to small movement of the boundary in the normal direction. In particular this implies that refining the mesh or/and taking a smaller time step, will not ensure, or will require an impractically fine grid to ensure, that each one-dimensional section of the domain satisfies requirement (3.2).

4 Convergence Analysis

In this section a convergence analysis is carried out for semi-discrete schemes.

4.1 Semi-Discrete Analysis

For the sake of analysis, we assume the following inner product is applied at each T_n:

$$(\,\cdot\,,\cdot\,)_n := \frac{\langle R_n(t)\,\cdot\,,\cdot\,\rangle}{N(n)} \quad \left(\|\cdot\|_n := \left((\,\cdot\,,\cdot\,)_n^{\frac{1}{2}}\right)\right), \quad R_n(t) \in Mat^{Sym}_{N(n)}, \tag{4.1}$$

where $R_n(t)$ is a Positive-Definite (**P.D**) piecewise constant matrix, $N(n)$ is the total number of internal and non-*suspended* grid-points at T_n, and $Mat^{Sym}_{N(n)}$ denotes the sub-space of $N(n) \times N(n)$ symmetric matrices.
Similar to the Constant Boundary case, we have

$$\frac{d}{dt}\boldsymbol{E} = M\boldsymbol{E} + \boldsymbol{T} \quad \forall\, t \in Tn, \tag{4.2}$$

where $\boldsymbol{E} := \boldsymbol{U} - \boldsymbol{V}\ \forall\ t \in Tn$. Accordingly, taking the inner product, $(\,\cdot\,,\cdot\,)_n$, of $\boldsymbol{E}$ with (4.2) yields

$$\begin{aligned} \frac{d}{dt}\left\|\boldsymbol{E}\right\|_n^2 &= (\boldsymbol{E}, M\boldsymbol{E})_n + (\boldsymbol{E}, \mathbf{T})_n & (4.3)\\ &\leq -c_n \cdot \left\|\boldsymbol{E}\right\|_n^2 + \left|(\boldsymbol{E}, \mathbf{T})_n\right|, & (4.4)\end{aligned}$$

where c_n is the minimal eigenvalue of $-\left[R_n M\right]^S$ at T_n,

$$c_\nu := -\max_{t_\nu \leq t \leq t_{\nu+1}} \left\{\sigma\left(\left[R_n M\right]^S\right)\right\}, \quad \nu = 0, 1, 2 \ldots n, \tag{4.5}$$

and $\left[R_n M\right]^S := \left(R_n M + \left[R_n M\right]^T\right)/2$. Using Schwartz's inequality, dividing by $\left\|\boldsymbol{E}\right\|_n$ and applying Gronwall's Lema, we get

$$\begin{aligned} \left\|\boldsymbol{E}(t)\right\|_n &\leq \left\|\boldsymbol{T}\right\|_{n,\infty} h^m \frac{1 - e^{-c_n(t-t_n)}}{c_n} + \left\|\boldsymbol{E}(t_n)\right\|_n e^{-c_n(t-t_n)}, & (4.6)\\ \left\|\boldsymbol{T}\right\|_{\nu,\infty} &:= \sup_{t \in T_\nu} \left\|\boldsymbol{T}\right\|_\nu / h^m. & (4.7)\end{aligned}$$

Note that, for $c_n = 0$, we take (4.6) as the limit of $c_n \to 0^+$,

$$\left\|\boldsymbol{E}(t)\right\|_n \leq \left\|\boldsymbol{T}\right\|_{n,\infty} h^m (t - t_n) + \left\|\boldsymbol{E}(t_n)\right\|_n. \tag{4.8}$$

Accordingly,

- The extrapolation step at the end of every T_n implies

$$\left\|\boldsymbol{E}(t_{\nu+1})\right\|_{\nu+1} \leq \left\|\boldsymbol{E}(t_{\nu+1})\right\|_\nu + \bar{\epsilon}_{\nu+1} \left|O\left(h^m\right)\right|, \tag{4.9}$$

  where $\bar{\epsilon}_\nu := \frac{\epsilon_\nu}{\sqrt{N(\nu)}}$, and ϵ_ν denotes the number of newly entering grid-points at t_ν.

- Similar to (4.6), we have

$$\left\|\boldsymbol{E}(t_{\nu+1})\right\|_\nu \leq \left\|\boldsymbol{T}\right\|_{\nu,\infty} h^m \frac{1 - e^{-c_\nu \cdot k}}{c_\nu} + \left\|\boldsymbol{E}(t_\nu)\right\|_\nu \cdot e^{-c_\nu \cdot k}. \tag{4.10}$$

Hence, (4.6) combined with (4.9) and (4.10) gives a *Recurrence* inequality with the following solution:

$$\left\|\boldsymbol{E}(t)\right\|_n \leq \sum_{\nu=1}^{n} \left[\left(\frac{\beta_\nu}{\alpha_\nu}\left\|\boldsymbol{T}\right\|_{n,\infty} h^m + \frac{\epsilon_\nu \cdot |O(h^m)|}{\sqrt{N(\nu)}}\right)\left(\prod_{\mu=\nu}^{n} \alpha_\mu\right)\right], \tag{4.11}$$

where

$$\alpha_\nu := \begin{cases} e^{-c_\nu \cdot k} & if \quad \nu < n \\ e^{-c_n \cdot (t-t_n)} & if \quad \nu = n \end{cases}, \quad \beta_\nu := \frac{1-\alpha_\nu}{c_\nu} \underset{c_\nu \to 0^+}{\to} \begin{cases} k & if \quad \nu < n, \\ t-t_n & if \quad \nu = n \end{cases}. \tag{4.12}$$

Indeed, we generally have

$$\begin{cases} c_\nu = 0 \quad \forall\, 0 \le \nu \le n & \text{if (2.6) is hyperbolic,} \\ c_\nu \ge \overline{c} > 0 \quad \forall\, 0 \le \nu \le n & \text{if (2.6) is parabolic.} \end{cases} \tag{4.13}$$

Thus,

$$\|\boldsymbol{E}(t)\|_n \;\le\; \begin{cases} \left(\|\boldsymbol{T}\|_\infty + \left|O\left(\frac{\overline{\epsilon}}{k}\right)\right|\right) \cdot h^m t & \text{if (2.6) is hyperbolic,} \\ \left(\|\boldsymbol{T}\|_\infty + \left|O\left(\frac{\overline{\epsilon}}{k}\right)\right|\right) \cdot h^m \frac{1-e^{-\overline{c}\cdot t}}{\overline{c}} & \text{if (2.6) is parabolic,} \end{cases} \tag{4.14}$$

where

$$\|\boldsymbol{T}\|_\infty := \max_{0 \le \nu \le n} \|\boldsymbol{T}\|_{\nu,\infty}, \quad \overline{\epsilon} := \max_{0 \le \nu \le n} \overline{\epsilon}_\nu. \tag{4.15}$$

4.2 Multi-Dimensional Considerations

In general, constructing matrices M and $R_n(t)$ in the event of Merger/Split, for which $\overline{c} \ge 0$, is easily done in the genuine one-dimensional case, but becomes excessively complicated in the multi-dimensional case.
Accordingly, for the multi-dimensional Case, we set $R_n(t) \equiv I$, but apply the numerical solution over $X_A(t)$, where $\boldsymbol{V}$ at *admissible suspended* grid-points is evaluated at every stage using extrapolation on neighboring boundary and grid-points. Note that, *admissible suspended* grid-points are always spatially proximate to the boundary in the multi-dimensional case, thus the extrapolated values are assured to have a small enough error.

5 General Scheme Analysis and Numerical Considerations

In this section, we underlay the notation and fundamental assumptions for analysis, and discuss some numerical considerations.

5.1 Fundamental Assumptions

Since we use one-dimensional problems as building blocks for a general multi-dimensional problems, we apply the analysis for a one-dimensional problem

at a time point $t \in T_n$, characterized by the following properties, as displayed in Figure 5.1:

- Two real boundaries: $\Gamma_1 := \Gamma_L(t)$ and $\Gamma_{q_f} := \Gamma_R(t)$,
- $q_f - 1$ mergers, which occurred before t,
- $\Gamma_q - \Gamma_{q-1} \gg \mathcal{S} \quad$ for $\quad q = 1, 2 \ldots q_f$,

where $\{\Gamma_q\}_1^{q_f-1}$ denote the boundary join points, and,

$$\gamma_L(t) \;:=\; \frac{x_1 - \Gamma_L(t)}{h}, \quad \gamma_R(t) \;:=\; \frac{\Gamma_R(t) - x_N}{h}, \tag{5.1}$$

where x_1 and x_N are the *admissible non-suspended* grid-points most spatially proximate to the boundary points Γ_L and Γ_R respectively.

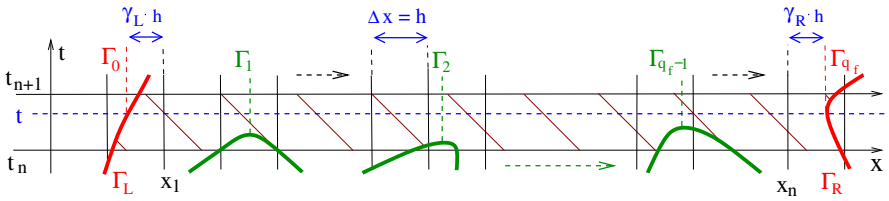

Figure 5.1: The General One-Dimensional Model

5.2 General Matrix Formulation

For Dirichlet boundary conditions, the general form of M is given by

$$M = L_N + \sum_{q=1}^{q_f-1} C_N^{(q)} - T_L A_L - T_R A_R, \tag{5.2}$$

where

- L_N, the *inner part of the scheme*, is a block-diagonal differentiation matrix

$$L_N = \begin{pmatrix} L_N^{(1)} & & & \\ & L_N^{(2)} & & \\ & & \ddots & \\ & & & L_N^{(q_f)} \end{pmatrix}, \tag{5.3}$$

and each block, $L_N^{(q)}$, is a differentiation sub-matrix applied over $X_I^{(q)}(t) := \{x_j \in X_I(t) \mid \Gamma_{q-1} < x_j < \Gamma_q\}$.

- $\left\{C_N^{(q)}\right\}_{q=1}^{q_f-1}$ are continuity operator applied over neighboring grid-points of Γ_q.

- T_L, T_R and A_L, A_R are diagonal weights matrices and boundary value extrapolation matrices respectively, for Dirichlet boundary conditions, as described in section 2.2.1,

$$T_L := \begin{pmatrix} \tau_L^{(1)} & & & \\ & \tau_L^{(2)} & & \\ & & \ddots & \\ & & & \tau_L^{(N)} \end{pmatrix}, \quad T_R := \begin{pmatrix} \tau_R^{(N)} & & & \\ & \tau_R^{(N-1)} & & \\ & & \ddots & \\ & & & \tau_R^{(1)} \end{pmatrix}, \tag{5.4}$$

$$A_L := \begin{pmatrix} a_L^{(1)} & \cdots & a_L^{(p_f)} & 0 & \cdots \\ a_L^{(1)} & \cdots & a_L^{(p_f)} & 0 & \cdots \\ \vdots & \ddots & \vdots & \vdots & \ddots \\ a_L^{(1)} & \cdots & a_L^{(p_f)} & 0 & \cdots \end{pmatrix}, \; A_R := \begin{pmatrix} \cdots & 0 & a_R^{(p_f)} & \cdots & a_R^{(1)} \\ \cdots & 0 & a_R^{(p_f)} & \cdots & a_R^{(1)} \\ \ddots & \vdots & \vdots & \ddots & \vdots \\ \cdots & 0 & a_R^{(p_f)} & \cdots & a_R^{(1)} \end{pmatrix}. \tag{5.5}$$

Though, in principle, the penalty terms $\left(A_{L/R}\boldsymbol{V} - \boldsymbol{G}_{L/R}\right)$ are added to each point, in practice, they are added just near the boundaries, i.e

$$\exists j_f \in \mathbb{N} \; : \; \tau_{L/R}^{(j)} = 0 \quad \forall \, j > j_f, \quad j_f \ll N(n). \tag{5.6}$$

5.3 Vanishing Boundaries and Continuity Operators

When a Merger event occurs at some time point $t^* \in T_n$, we replace the relevant numerical boundary operator with a requirement of continuity along ghost-points, which represent extensions of the vanishing boundaries.

For simplicity, we implement the continuity operator by setting some local differentiation operator for $t > t^*$, which is equivalent to a requirement for solution continuity along discontinuous, and perpendicular to the x-axis ghost-points extensions, as displayed in Figure 5.2.

6 Application: the Diffusion Equation

In this section, we analyze and construct numerical schemes of the diffusion equation for both 2^{nd}-order and 4^{th}-order approximations. The analysis is

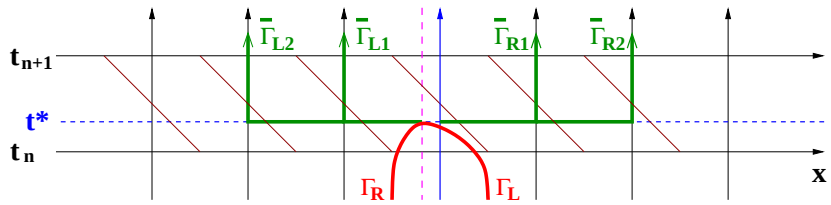

Figure 5.2: Vanishing Boundaries Discontinuous Extension

applied to a one-dimensional normalized equation, with Dirichlet boundary conditions,

$$\frac{\partial u}{\partial t} = \frac{\partial^2 u}{\partial x^2} + f(x,t), \tag{6.1}$$

$$u(x,0) = u_0(x), \tag{6.2}$$

$$u(\Gamma_{L/R}(t),t) = g_{L/R}(t), \tag{6.3}$$

such that $\Omega(t) \subset [0,1]$, $\forall\, t \geq 0$.

6.1 2nd-Order Approximation

For the 2nd-order case, we have (see section 5.2)

$$L_N^{(q)} := \frac{1}{h^2}\begin{pmatrix} 1 & -2 & 1 & & & & \\ 1 & -2 & 1 & & & & \\ & 1 & -2 & 1 & & & \\ & & & \ddots & & & \\ & & & 1 & -2 & 1 & \\ & & & & 1 & -2 & 1 \\ & & & & 1 & -2 & 1 \end{pmatrix}, \tag{6.4}$$

where a 2nd-order symmetric approximation to $\frac{\partial^2}{\partial x^2}$ is used at internal points, and a 1st-order (not symmetric) approximation to $\frac{\partial^2}{\partial x^2}$ is used near the edges. Note that, the lower accuracy near the edges does not affect the overall accuracy, as does the order of the imposed boundary conditions that are one less than that of the inner scheme (see [32], [33], [34] for details).

By setting $p = 3$, we have

$$\begin{aligned} a_{L/R}^{(1)} &:= \frac{1}{2}(\gamma_{L/R}+1)(\gamma_{L/R}+2), \\ a_{L/R}^{(2)} &:= -\gamma_{L/R}(\gamma_{L/R}+2), \\ a_{L/R}^{(3)} &:= \frac{1}{2}\gamma_{L/R}(\gamma_{L/R}+1), \end{aligned}$$

and, for $j_f = 1$, we may designate

$$\tau_{L/R}^{(1)} := \frac{1}{h^2} \cdot \frac{-3\gamma_{L/R}+9}{(\gamma_{L/R}+1)(\gamma_{L/R}+2)} \quad \left(\tau_{L/R}^{(j)} = 0 \; \forall j > j_f = 1\right). \tag{6.5}$$

Hence, the general form of the matrix, becomes as displayed in Figure 6.1.

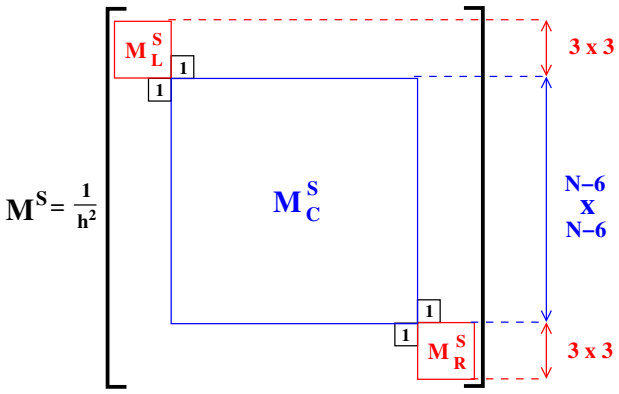

Figure 6.1: General Matrix Form - 2nd-Order

Accordingly, for the eigenvalues bound analysis, we define two matrices, $D_2^{(0)}$ and $D_2^{(1)}$,

$$D_2^{(0)} := \begin{pmatrix} -1 & 1 & & & \\ 1 & -2 & 1 & & \\ & \ddots & \ddots & \ddots & \\ & & 1 & -2 & 1 \\ & & & 1 & -1 \end{pmatrix}, \; D_2^{(1)} := \begin{pmatrix} -2 & 1 & & & \\ 1 & -2 & 1 & & \\ & \ddots & \ddots & \ddots & \\ & & 1 & -2 & 1 \\ & & & 1 & -2 \end{pmatrix}, \tag{6.6}$$

where $D_2^{(1)}$ is N.D, and $D_2^{(0)}$ is N.P.D with the eigenvalue 0 of algebraic multiplicity 1 (see appendix A for details).

6.1.1 Case 1: No Merger

For this case, no Merger took place $\forall\, t^* \in (t_n, t)$, hence no continuity operators are applied. Accordingly, it can be easily verified that

$$\varepsilon_m(\gamma_L, \gamma_R) \;:=\; \sup\left\{\varepsilon \in (0,1) \;\middle|\; M^S - \frac{1}{h^2}\left[\varepsilon D_2^{(1)} + (1-\varepsilon)\overline{D}_2^{(0)}\right] \le 0\right\} \tag{6.7}$$

satisfies

$$\varepsilon_m(\gamma_L, \gamma_R) > \frac{12}{25} \quad \forall\, (\gamma_L, \gamma_R) \in [0, 3/2] \times [0, 3/2], \tag{6.8}$$

where the matrix $\overline{D}_2^{(0)}$ is set by positioning the blocks $\left[\phi_2, D_2^{(0)}, \phi_2\right]$ along the main diagonal, as displayed in Figure 6.2, and ϕ_ν denotes a $\nu \times \nu$ zeros matrix.

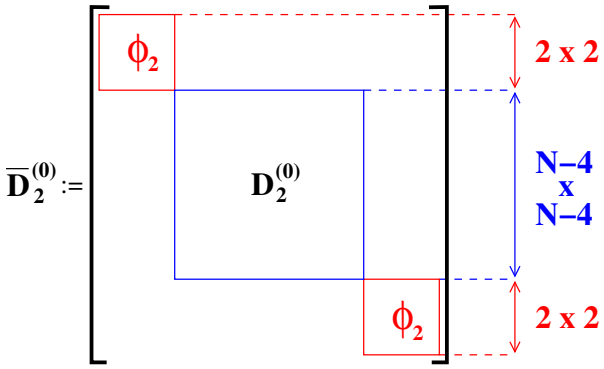

Figure 6.2: The $\overline{D}_2^{(0)}$ Matrix - 2^{nd}-Order

Consequently, since $D_2^{(0)}$ is N.P.D then $\overline{D}_2^{(0)}$ is N.P.D as well, then c_n, the minimal eigenvalue of $-M^S$ at T_n, satisfies (see appendix A for details)

$$c_n \;=\; -\max_{t_n \le t \le t_{n+1}} \left\{\sigma\left(M^S\right)\right\} \;\ge\; -\varepsilon_m \max\left\{\sigma\left(\frac{1}{h^2} D_2^{(1)}\right)\right\} \;>\; 12\left(\frac{\pi}{5}\right)^2. \tag{6.9}$$

6.1.2 Case 2: Mergers without Entering Grid-Points

For a single Merger, as displayed in Figure 6.3, we apply

- Boundary operators in the neighborhood of Γ_{join}, for $t_n < t < t^*$.
- Continuity operators at the neighborhood of Γ_{join}, for $t^* < t < t_{n+1}$.

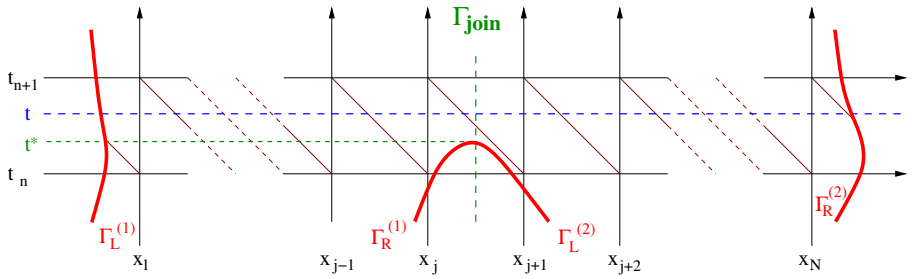

Figure 6.3: Merger Without an Entering Grid-Point

Accordingly, we embed the continuity operators along ghost-points at x_{j-1} and x_{j+1} in the following manner:

$$[L_N \boldsymbol{V}]_j \;-\; \tau_R^{(1)}\Big|_{\gamma_R=1}\left[\left(a_R^{(3)}\cdot v_{j-2}+a_R^{(2)}\cdot v_{j-1}+a_R^{(1)}\cdot v_j\right)\Big|_{\gamma_R=1}-v_{j+1}\right], \tag{6.10}$$

$$[L_N \boldsymbol{V}]_{j+1} \;-\; \tau_L^{(1)}\Big|_{\gamma_L=1}\left[\left(a_L^{(3)}\cdot v_{j+3}+a_L^{(2)}\cdot v_{j+2}+a_L^{(1)}\cdot v_{j+1}\right)\Big|_{\gamma_L=1}-v_j\right], \tag{6.11}$$

where $[\boldsymbol{W}]_i$ denotes the i^{th} coordinate of the vector $\boldsymbol{W}$, and get

$$\frac{d}{dt}v_j=\frac{v_{j-1}-2v_j+v_{j+1}}{h^2},\quad \frac{d}{dt}v_{j+1}=\frac{v_j-2v_{j+1}+v_{j+2}}{h^2}. \tag{6.12}$$

Hence, regardless to the number of Mergers, the minimal eigenvalue analysis of the matrix $-M^S$ remains identical to Case 1:

$$M_C^S \;=\; D_2^{(1)} \quad\Rightarrow\quad c_n \;:=\; -\max_{t_n\le t\le t_{n+1}}\left\{\sigma\left(M^S\right)\right\} \;>\; 12\left(\frac{\pi}{5}\right)^2. \tag{6.13}$$

6.1.3 Case 3: Mergers with Entering Grid-Points

Considering a single Merger with a single entering grid-point, x_j, as displayed in Figure 6.4, we apply, without the loss of generality, the continuity operator on $\kappa \ll N_{L/R}$ grid-points to the left and to the right of x_j. Hence, in the general matrix form ,M_C^S, is as displayed in Figure 6.5.

We are going to show that, in this case, the assumptions so far lead inevitably to indefiniteness of M^S in the standard norm, $\langle\cdot,\cdot\rangle^{1/2}$.
Indeed showing that M_C^S, the central block of the matrix M^S, is indefinite, implies that M^S is also indefinite regardless of the choice of the boundary

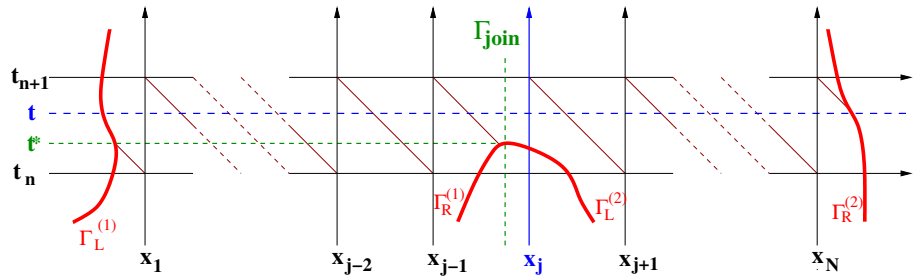

Figure 6.4: Merger With an Entering Grid-Point

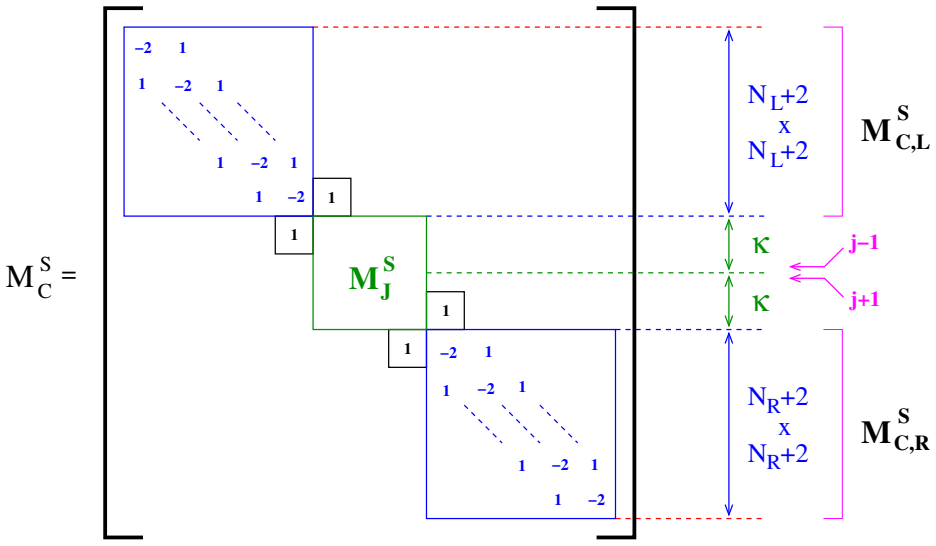

Figure 6.5: Case 3 General Matrix Form - 2nd-Order

terms. The inequality analysis employed in Case 1 is not subtle enough, and, for this case, we employ a more accurate analysis in the following sub-sections.

Isolation by Congruence Equivalency

In this sub-section, we seek a symmetric matrix, $\overline{M}_C^S$, congruent with M_C^S,

$$M_C^S = C^T \overline{M}_C^S C, \quad \det(C) \neq 0, \tag{6.14}$$

such that the local differentiation block, M_J^S, becomes isolated. Accordingly, we set the congruence matrix, C, as displayed in Figure 6.6:

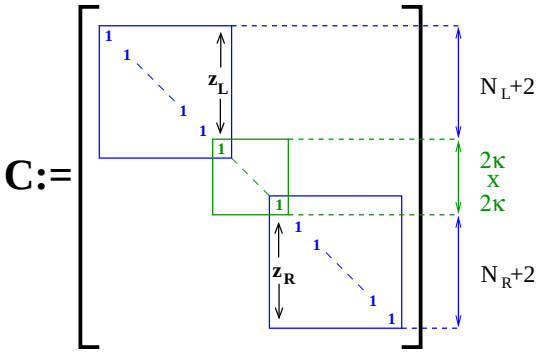

Figure 6.6: The Congruence Matrix - 2nd-Order

where the elements of the columns,

$$\boldsymbol{z}_L := \left(z_L^{(N_L)}, z_L^{(N_L-1)}, \dots z_L^{(-1)}\right)^T, \tag{6.15}$$

$$\boldsymbol{z}_R := \left(z_R^{(-1)}, z_R^{(0)}, \dots z_R^{(N_R)}\right)^T, \tag{6.16}$$

are determined uniquely by solving the difference equation,

$$z_{L/R}^{(j)} = 2z_{L/R}^{(j-1)} - z_{L/R}^{(j-2)} \ , \ j \in \{1, 2, \dots N_{L/R}\}, \tag{6.17}$$

constrained by the following initial and terminal conditions:

$$-2z_{L/R}^{(-1)} + z_{L/R}^{(0)} = 1, \tag{6.18}$$

$$-2z_{L/R}^{(N_{L/R})} + z_{L/R}^{(N_{L/R}-1)} = 0. \tag{6.19}$$

Accordingly, the congruent matrix, $\overline{M}_C^S = \left(C^{-1}\right)^T M_C^S C^{-1}$, takes the form as displayed in Figure 6.7, where the *corner supplements*, $\delta_{L/R}$, are given by

$$\delta_{L/R} = -z_{L/R}^{(-1)} = \frac{(N_{L/R}+1)+1}{(N_{L/R}+2)+1} \approx 1 - \frac{1}{N_{L/R}+2}. \tag{6.20}$$

The Fixed Sub-Space Property of M_J

By definition M_J is a $2\kappa \times 2\kappa$ differentiation sub-matrix, applied over a uniform mesh with a missing grid-point. Hence, for any $\kappa \in \mathbb{N}$, it satisfies

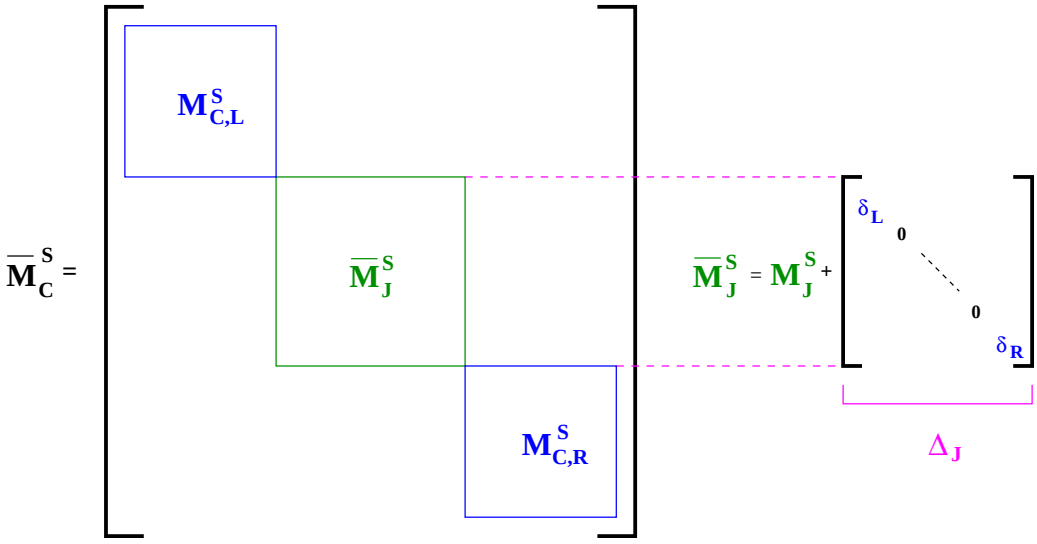

Figure 6.7: The Congruent Central Matrix - 2^{nd}-Order

the following relation:

$$\begin{pmatrix} 1 & & \\ & M_J & \\ & & 1 \end{pmatrix} \boldsymbol{w}_i^{\kappa+1} = \begin{cases} \mathbf{0} & if \quad i = 0,1 \\ i \cdot (i-1) \cdot \boldsymbol{w}_{i-2}^{\kappa} & if \quad i = 2,3 \end{cases} \tag{6.21}$$

where $\boldsymbol{w}_i^l := \left((-l)^i, (-l+1)^i, \ldots (-1)^i, 1, 2^i, \ldots (l-1)^i, l^i\right)^T$.
This implies that any M_J we may designate satisfies

$$\forall\, \boldsymbol{w} \in W_4^{\kappa} \quad \exists\, !\widetilde{\boldsymbol{w}} \in \mathbb{R}^{2\kappa} \;:\; M_J \boldsymbol{w} = \widetilde{\boldsymbol{w}}, \tag{6.22}$$

where

$$W_p^l := Span\left\{\boldsymbol{w}_0^l, \boldsymbol{w}_1^l, \boldsymbol{w}_2^l, \ldots \boldsymbol{w}_{p-1}^l\right\}. \tag{6.23}$$

Conclusion: Indefiniteness of M^S

By denoting $\varepsilon_{L/R} := 1 - \delta_{L/R}$, we get from (6.20) that $\varepsilon_{L/R} \approx \frac{1}{N_{L/R}+2}$, and, by choosing the vector,

$$\boldsymbol{w}^* := -\sqrt{\frac{8}{3}}\kappa^{5/2}\boldsymbol{w}_0^{\kappa} + \sqrt{\frac{3}{2}}\kappa^{-1/2}\boldsymbol{w}_2^{\kappa} \;\in\; W_4^{\kappa}, \tag{6.24}$$

we have, using (6.22),

$$\left\langle \boldsymbol{w}^* \, , \overline{M}_J^S \boldsymbol{w}^* \right\rangle = \left\langle \boldsymbol{w}^* \, , \left[M_J + \overline{\Delta}_J \right] \boldsymbol{w}^* \right\rangle = 1 + O\left(\kappa^5 \left(\bar{\varepsilon}_L + \bar{\varepsilon}_R \right) \right) . \quad (6.25)$$

Hence, a construction of a N.D matrix, M, is not feasible under the assumptions so far.

Solution: Local Norm Modifications

For a genuine one-dimensional problem, we may set a norm associated with the matrix $R_n(t)$, that applies local modification blocks, R, on M_J blocks along the main diagonal as displayed in Figure 6.8,

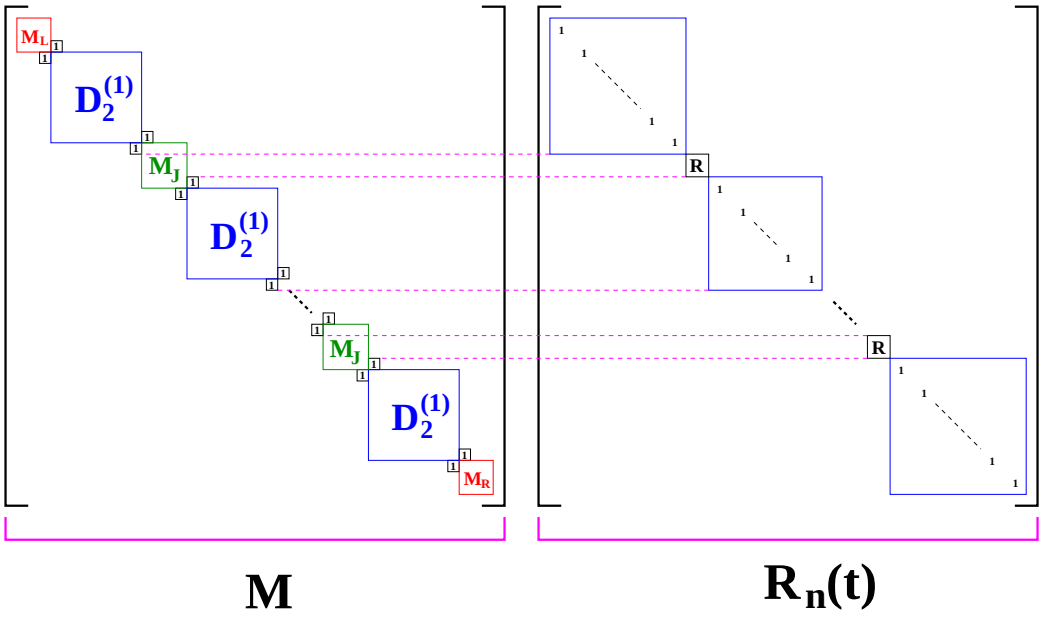

Figure 6.8: The Norm Matrix - 2nd-Order

where, for a $2\kappa \times 2\kappa$ M_J block, R is set as a $2(\kappa-1) \times 2(\kappa-1)$ block. Indeed, we set $\kappa = 3$, and

$$R := \begin{pmatrix} 1 & & & \\ & 5/4 & 1/4 & \\ & 1/4 & 5/4 & \\ & & & 1 \end{pmatrix} > 0 \quad , \quad R \in Mat_4^{Sym}, \quad (6.26)$$

which satisfies $\langle \boldsymbol{V}_J, R\boldsymbol{V}_J \rangle = \langle \overline{\boldsymbol{V}}_J, \overline{\boldsymbol{V}}_J \rangle$, where

$$\boldsymbol{V}_J := (v_{-2}, v_{-1}, v_1, v_2)^T , \quad \overline{\boldsymbol{V}}_J := \left(v_{-2}, v_{-1}, \frac{v_{-1}+v_1}{2}, v_1, v_2 \right)^T . \quad (6.27)$$

Thus, by setting

$$M_J := \begin{pmatrix} -2 & 1 & & & & \\ 1 & -2 & 1 & & & \\ & 5/6 & -4/3 & 2/3 & -1/6 & \\ & -1/6 & 2/3 & -4/3 & 5/6 & \\ & & & 1 & -2 & 1 \\ & & & & 1 & -2 \end{pmatrix}, \tag{6.28}$$

we get that the minimal eigenvalue analysis of the matrix $-M^S$ remains identical to Case 1:

$$c_n := -\max_{t_n \le t \le t_{n+1}} \left\{ \sigma\left([R_n M]^S \right) \right\} \ge -\overline{\varepsilon}_m \max\left\{ \sigma\left(\frac{1}{h^2} D_2^{(1)} \right) \right\} > 12\left(\frac{\pi}{5}\right)^2, \tag{6.29}$$

where $[R_n M]^S := \left([R_n M] + [R_n M]^T \right)/2$, $\overline{\varepsilon}_m$ is defined by

$$\overline{\varepsilon}_m := \sup\left\{ \varepsilon \in (0,1) \;\middle|\; [R_n M]^S - \frac{1}{h^2}\left[\varepsilon D_2^{(1)} - (1-\varepsilon)\overline{\overline{D}}_2^{(0)} \right] \le 0 \right\} = \varepsilon_m, \tag{6.30}$$

and the matrix $\overline{\overline{D}}_2^{(0)}$ is set by positioning $\left[\phi_2, D_2^{(0)}, \phi_4, D_2^{(0)}, \ldots \phi_4, D_2^{(0)}, \phi_2\right]$ blocks along the main diagonal, as displayed in Figure 6.9.

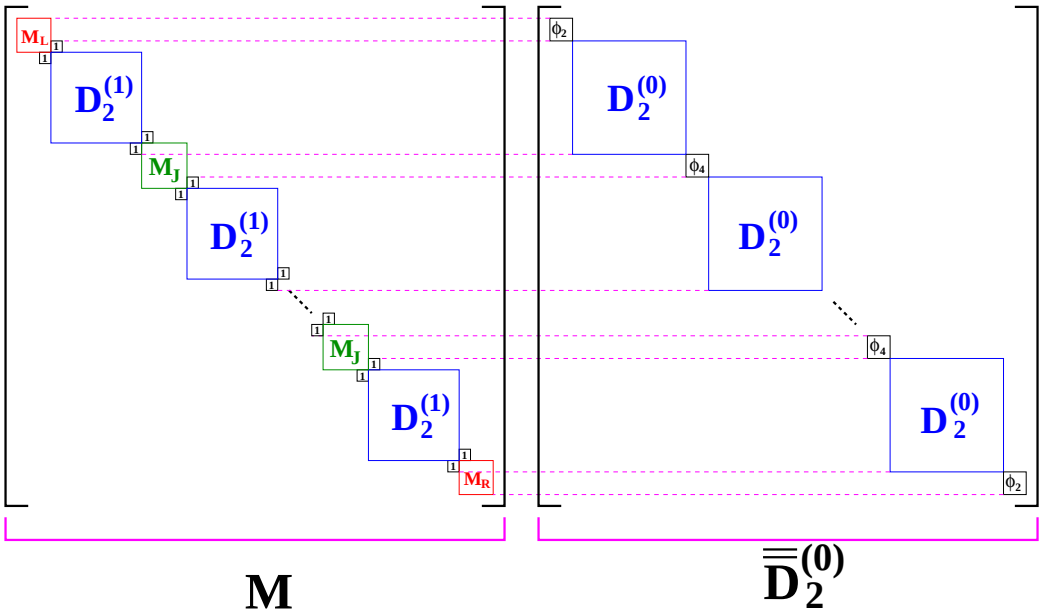

Figure 6.9: The $\overline{\overline{D}}_2^{(0)}$ Matrix - 2nd-Order

6.2 4^{th}-Order Approximation

For the 4^{th}-order case, we apply a 4^{th}-order symmetric approximation at internal points, and a 3^{rd}-order (not symmetric) approximation near the edges,

$$L_N^{(q)} := \frac{1}{12h^2}\begin{pmatrix} 35 & -104 & 114 & -56 & 11 & 0 & 0 & \cdots & & 0 \\ 11 & -20 & 6 & 4 & -1 & 0 & 0 & \cdots & & 0 \\ -1 & 16 & -30 & 16 & -1 & 0 & 0 & \cdots & & 0 \\ 0 & -1 & 16 & -30 & 16 & -1 & 0 & \cdots & & 0 \\ \vdots & & \ddots & & & \ddots & & \ddots & & \vdots \\ 0 & & \cdots & & 0 & -1 & 16 & -30 & 16 & -1 & 0 \\ 0 & & \cdots & & 0 & 0 & -1 & 16 & -30 & 16 & -1 \\ 0 & & \cdots & & 0 & 0 & -1 & 4 & 6 & -20 & 11 \\ 0 & & \cdots & & 0 & 0 & 11 & -56 & 114 & -104 & 35 \end{pmatrix}, \tag{6.31}$$

where $L_N^{(q)}$ is a differentiation sub-matrix as described in section 5.2.
By setting $p = 5$, we have the following extrapolation to the boundary coefficients:

$$\begin{aligned} a_{L/R}^{(1)} &:= \frac{1}{24}(\gamma_{L/R}+1)(\gamma_{L/R}+2)(\gamma_{L/R}+3)(\gamma_{L/R}+4), \\ a_{L/R}^{(2)} &:= -\frac{1}{6}\gamma_{L/R}(\gamma_{L/R}+2)(\gamma_{L/R}+3)(\gamma_{L/R}+4), \\ a_{L/R}^{(3)} &:= \frac{1}{4}\gamma_{L/R}(\gamma_{L/R}+1)(\gamma_{L/R}+3)(\gamma_{L/R}+4), \\ a_{L/R}^{(4)} &:= -\frac{1}{6}\gamma_{L/R}(\gamma_{L/R}+1)(\gamma_{L/R}+2)(\gamma_{L/R}+4), \\ a_{L/R}^{(5)} &:= \frac{1}{24}\gamma_{L/R}(\gamma_{L/R}+1)(\gamma_{L/R}+2)(\gamma_{L/R}+3), \end{aligned}$$

and, for $j_f = 2$, we may designate the following weights:

$$\tau_{L/R}^{(1)} := \frac{1}{h^2}\cdot\frac{220\gamma_{L/R}^2 - 520\gamma_{L/R} + 400}{(\gamma_{L/R}+1)(\gamma_{L/R}+2)(\gamma_{L/R}+3)(\gamma_{L/R}+4)}, \tag{6.32}$$

$$\tau_{L/R}^{(2)} := \frac{1}{h^2}\cdot\frac{-100\gamma_{L/R}^2 + 200\gamma_{L/R} - 110}{(\gamma_{L/R}+1)(\gamma_{L/R}+2)(\gamma_{L/R}+3)(\gamma_{L/R}+4)}. \tag{6.33}$$

$$\left(\tau_{L/R}^{(j)} = 0 \quad \forall\, j > j_f\right)$$

Hence, the general form of the matrix, becomes as displayed in Figure 6.10.

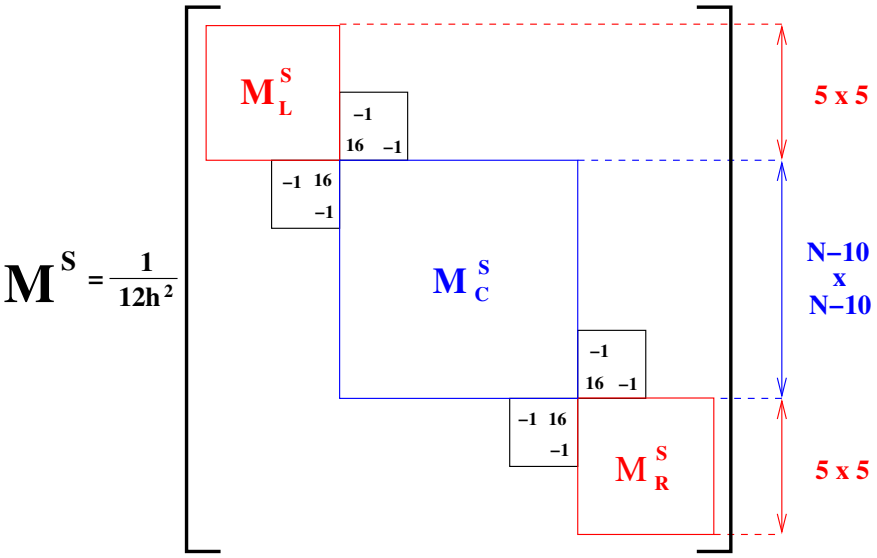

Figure 6.10: General Matrix Form - 4th-Order

Accordingly, we define two matrices, $D_4^{(0)}$ and $D_4^{(1)}$, analogously to the 2nd-order case as displayed in Figure 6.11,

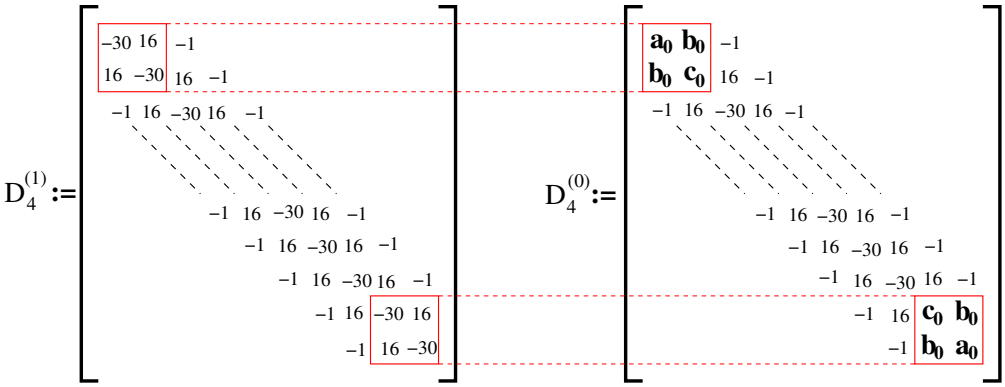

Figure 6.11: The Fundamental Matrices - 4th-Order

where $D_4^{(1)}$ is N.D, and the corners of $D_4^{(0)} \in Mat_{N_0}^{Sym}$ are set by

$$\begin{pmatrix} a_0 & b_0 \\ b_0 & c_0 \end{pmatrix} = \begin{pmatrix} -7+4\sqrt{3} & 8-4\sqrt{3} \\ 8-4\sqrt{3} & -23+4\sqrt{3} \end{pmatrix} - \frac{8\sqrt{3}}{\left(7+4\sqrt{3}\right)^{N_0-2}} \begin{pmatrix} 1 & -1 \\ -1 & 1 \end{pmatrix}, \tag{6.34}$$

which assures that $D_4^{(0)}$ is N.P.D, with the eigenvalue 0 of algebraic

multiplicity 2 (see appendix A for details).

6.2.1 Case 1: No Merger

As in the 2nd-order case, no continuity operators are applied, and it can be easily verified that

$$\varepsilon_m(\gamma_L,\gamma_R) \;:=\; \sup\left\{\varepsilon\in(0,1)\;\middle|\; M^S-\frac{1}{12h^2}\left[\varepsilon D_4^{(1)}+(1-\varepsilon)\overline{D}_4^{(0)}\right]\;\leq 0\right\} \tag{6.35}$$

satisfies, for all $N>15$,

$$\varepsilon_m(\gamma_L,\gamma_R)>\frac{1}{25}\quad\forall\,(\gamma_L,\gamma_R)\in[0,3/2]\times[0,3/2], \tag{6.36}$$

where the matrix $\overline{D}_4^{(0)}$ is set by positioning the blocks $\left[\phi_3, D_4^{(0)}, \phi_3\right]$ along the main diagonal, as displayed in Figure 6.12.

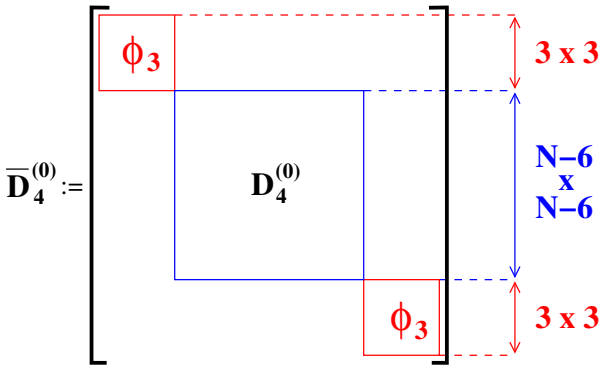

Figure 6.12: The $\overline{D}_4^{(0)}$ Matrix - 4th-Order

Accordingly, since $D_4^{(0)}$ is N.P.D, then $\overline{D}_4^{(0)}$ is N.P.D as well, thus c_n, the minimal eigenvalue of $-M^S$ at T_n, satisfies (see appendix A for details)

$$c_n \;:=\; -\max_{t_n\leq t\leq t_{n+1}}\left\{\sigma\left(M^S\right)\right\}\;\geq\;-\varepsilon_m\max\left\{\sigma\left(\frac{1}{12h^2}D_4^{(1)}\right)\right\}\;>\;\left(\frac{\pi}{5}\right)^2. \tag{6.37}$$

6.2.2 Case 2: Mergers without Entering Grid-Points

For a single Merger, as in the 2nd-order case we apply

- Boundary operators at the neighborhood of Γ_{join}, for $t_n<t<t^*$.

- Continuity operator at the neighborhood of Γ_{join}, for $t^* < t < t_{n+1}$.

By setting the continuity operator, represented as embedded continuity along ghost-points at x_{j-2}, x_{j-1}, x_{j+1} and x_{j+2}, in the following manner:

$$\begin{aligned}
[L_N \boldsymbol{V}]_{j-1} &- \tau_R^{(2)}\Big|_{\gamma_R=1} \left[\left(\sum_{p=1}^{5} a_R^{(p)} \cdot v_{j+1-p} \right) \Bigg|_{\gamma_R=1} - v_{j+1} \right] \\
&= \frac{-v_{j-3} + 16v_{j-2} - 30v_{j-1} + 16v_j - v_{j+1}}{12h^2}, \qquad (6.38)
\end{aligned}$$

$$\begin{aligned}
[L_N \boldsymbol{V}]_{j} &- \frac{16}{12h^2} \left[\left(\sum_{p=1}^{5} a_R^{(p)} \cdot v_{j+1-p} \right) \Bigg|_{\gamma_R=1} - v_{j+1} \right] \\
&+ \frac{1}{12h^2} \left[\left(\sum_{p=1}^{5} a_R^{(p)} \cdot v_{j+1-p} \right) \Bigg|_{\gamma_R=2} - v_{j+2} \right] \\
&= \frac{-v_{j-2} + 16v_{j-1} - 30v_j + 16v_{j+1} - v_{j+2}}{12h^2}, \qquad (6.39)
\end{aligned}$$

$$\begin{aligned}
[L_N \boldsymbol{V}]_{j+1} &- \frac{16}{12h^2} \left[\left(\sum_{p=1}^{5} a_L^{(p)} \cdot v_{j+p} \right) \Bigg|_{\gamma_R=1} - v_{j} \right] \\
&+ \frac{1}{12h^2} \left[\left(\sum_{p=1}^{5} a_L^{(p)} \cdot v_{j+p} \right) \Bigg|_{\gamma_R=2} - v_{j-1} \right] \\
&= \frac{-v_{j-1} + 16v_{j} - 30v_{j+1} + 16v_{j+2} - v_{j+3}}{12h^2}, \qquad (6.40)
\end{aligned}$$

$$\begin{aligned}
[L_N \boldsymbol{V}]_{j+2} &- \tau_L^{(2)}\Big|_{\gamma_L=1} \left[\left(\sum_{p=1}^{5} a_L^{(p)} \cdot v_{j+p} \right) \Bigg|_{\gamma_L=1} - v_{j-1} \right] \\
&= \frac{-v_{j} + 16v_{j+1} - 30v_{j+2} + 16v_{j+3} - v_{j+4}}{12h^2}, \qquad (6.41)
\end{aligned}$$

we get that the minimal eigenvalue analysis of the matrix $-M^S$ remains identical to Case 1:

$$M_C^S = D_4^{(1)} \quad \Rightarrow \quad c_n := -\max_{t_n \le t \le t_{n+1}} \left\{ \sigma\left(M^S\right) \right\} > \left(\frac{\pi}{5}\right)^2. \qquad (6.42)$$

6.2.3 Case 3: Mergers with Entering Grid-Points

As in the 2nd-order case, we consider a single Merger with a single entering grid-point, x_j, and apply the continuity operator on κ grid-points to the left and to the right of x_j, as shown in Figure 6.13.

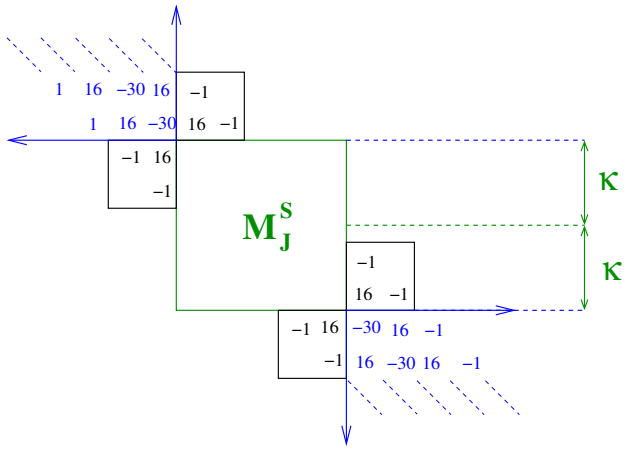

Figure 6.13: Case 3 General Matrix Form - 4th-Order

Indeed, applying similar analysis to the 2nd-order case, we get that the assumption $\kappa \ll N_{L/R}$ and previous assumptions lead inevitably to indefiniteness of M^S in the standard norm.

Isolation by Congruence Equivalency

To Isolate the local block, M_J^S, we apply a congruence transformation, $M_C^S = C^T \overline{M}_C^S C$, with the congruence matrix given in Figure 6.14.
The elements of the columns,

$$\boldsymbol{z}_{Li} := \left(z_{Li}^{(N_L)}, z_{Li}^{(N_L-1)}, \dots z_{Li}^{(-2)}, z_{Li}^{(-3)}\right)^T, \tag{6.43}$$

$$\boldsymbol{z}_{Ri} := \left(z_{Ri}^{(-3)}, z_{Ri}^{(-2)}, \dots z_{Ri}^{(N_R-1)}, z_{Ri}^{(N_R)}\right)^T, \tag{6.44}$$

are determined uniquely by solving a difference equation,

$$z_{Li/Ri}^{(j)} = 16 z_{Li/Ri}^{(j-1)} - 30 z_{Li/Ri}^{(j-2)} + 16 z_{Li/Ri}^{(j-3)} - z_{Li/Ri}^{(j-4)}\ ,\ j \in \{1, 2, \dots N_{L/R}\}, \tag{6.45}$$

with the following initial conditions:

$$-z_{Li/Ri}^{(-1)} + 16 z_{Li/Ri}^{(-2)} - 30 z_{Li/Ri}^{(-3)} = \begin{cases} 16 & \text{if} \quad i = 1 \\ -1 & \text{if} \quad i = 2 \end{cases}, \tag{6.46}$$

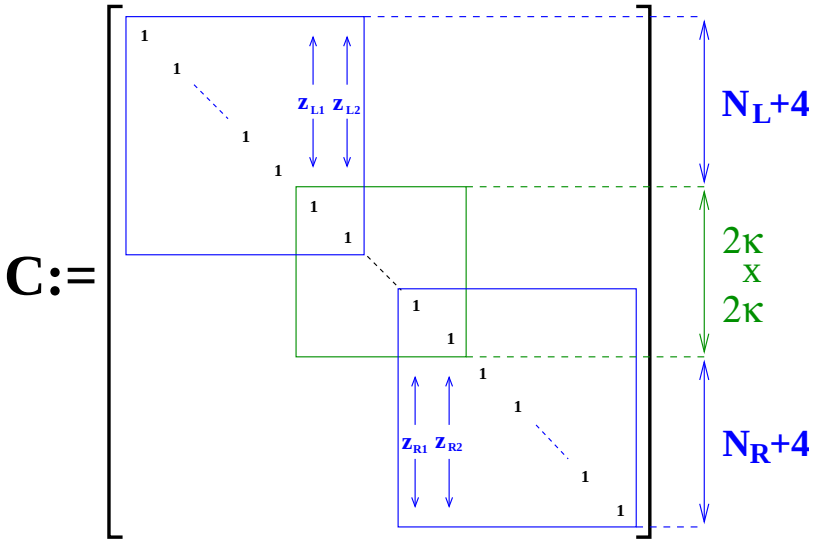

Figure 6.14: The Congruence Matrix - 4^{th}-Order

$$-z^{(0)}_{Li/Ri} + 16z^{(-1)}_{Li/Ri} - 30z^{(-2)}_{Li/Ri} + 16z^{(-3)}_{Li/Ri} = \begin{cases} -1 & \text{if} \quad i = 1 \\ 0 & \text{if} \quad i = 2 \end{cases}, \tag{6.47}$$

and the following terminal conditions:

$$-30z^{(N_{L/R})}_{Li/Ri} + 16z^{(N_{L/R}-1)}_{Li/Ri} - z^{(N_{L/R}-2)}_{Li/Ri} = 0, \tag{6.48}$$

$$16z^{(N_{L/R})}_{Li/Ri} - 30z^{(N_{L/R}-1)}_{Li/Ri} + 16z^{(N_{L/R}-2)}_{Li/Ri} - z^{(N_{L/R}-3)}_{Li/Ri} = 0. \tag{6.49}$$

This choice yields a congruent form as displayed in Figure 6.15, where the *corner supplements*, $\Delta_{L/R}$, are 2×2 P.D symmetric matrices, satisfying

$$\Delta_L \approx \begin{pmatrix} 23 - 4\sqrt{3} & -8 + 4\sqrt{3} \\ -8 + 4\sqrt{3} & 7 - 4\sqrt{3} \end{pmatrix} - \frac{1}{N_L + 4} \begin{pmatrix} 7 + 4\sqrt{3} & -1 \\ -1 & 7 - 4\sqrt{3} \end{pmatrix}, \tag{6.50}$$

and

$$\Delta_R \approx \begin{pmatrix} 7 - 4\sqrt{3} & -8 + 4\sqrt{3} \\ -8 + 4\sqrt{3} & 23 - 4\sqrt{3} \end{pmatrix} - \frac{1}{N_R + 4} \begin{pmatrix} 7 - 4\sqrt{3} & -1 \\ -1 & 7 + 4\sqrt{3} \end{pmatrix}. \tag{6.51}$$

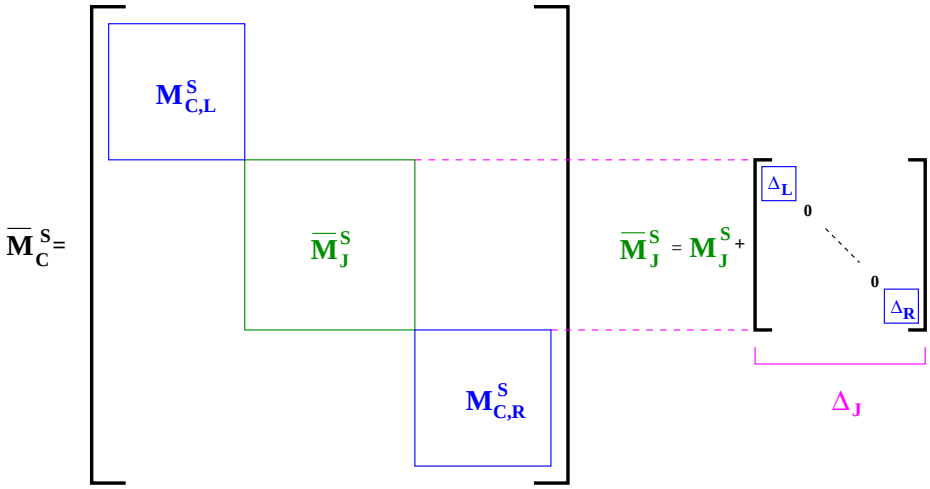

Figure 6.15: The Congruent Central Matrix - 4^{th}-Order

Conclusion: Indefiniteness of M^S

Applying similar analysis to the 2nd-order case, it can be shown that any M_J we may designate satisfies

$$\forall\, \boldsymbol{w} \in W_5^{\kappa} \quad \exists\, !\widetilde{\boldsymbol{w}} \in \mathbb{R}^{2\kappa} \;:\; M_J \boldsymbol{w} = \widetilde{\boldsymbol{w}}, \tag{6.52}$$

where W_5^{κ} is as defined in (6.23). So, by denoting

$$E_L \;:=\; \Delta_L - \begin{pmatrix} 23-4\sqrt{3} & -8+4\sqrt{3} \\ -8+4\sqrt{3} & 7-4\sqrt{3} \end{pmatrix}, \tag{6.53}$$

$$E_R \;:=\; \Delta_R - \begin{pmatrix} 7-4\sqrt{3} & -8+4\sqrt{3} \\ -8+4\sqrt{3} & 23-4\sqrt{3} \end{pmatrix}, \tag{6.54}$$

we have

$$\left\langle \boldsymbol{w}^* \,, \overline{M}_J^S \boldsymbol{w}^* \right\rangle = \left\langle \boldsymbol{w}^* \,, \left[M_J + \overline{\Delta}_J \right] \boldsymbol{w}^* \right\rangle = 1 + O\left(\kappa^6 \left(\overline{\varepsilon}_L + \overline{\varepsilon}_R \right) \right), \tag{6.55}$$

where

$$\boldsymbol{w}^* \;:=\; \left(\frac{16}{6-4\sqrt{3}} \kappa^3 - 4\kappa^2 + 4\kappa + \frac{3+94\sqrt{3}}{144} \right) \boldsymbol{w}_0^{\kappa} + \left(6+4\sqrt{3} \right) \boldsymbol{w}_2^{\kappa} \;\in\; W_5^{\kappa}, \tag{6.56}$$

and

$$\varepsilon_L \;:=\; \sup \left\{ \varepsilon \in (0,1) \,\middle|\, E_L + \varepsilon \begin{pmatrix} 7+4\sqrt{3} & -1 \\ -1 & 7-4\sqrt{3} \end{pmatrix} \geq 0 \right\} \approx \frac{1}{N_L+4}$$

$$\varepsilon_R \;:=\; \sup \left\{ \varepsilon \in (0,1) \,\middle|\, E_R + \varepsilon \begin{pmatrix} 7-4\sqrt{3} & -1 \\ -1 & 7+4\sqrt{3} \end{pmatrix} \geq 0 \right\} \approx \frac{1}{N_R+4}$$

Hence, a construction of a N.D matrix M is not feasible under the assumptions so far.

Solution: Local Norm Modifications

For a genuine one-dimensional problem we may set a norm associated with the matrix $R_n(t)$ that applies local modifications on M_J blocks along the main diagonal, as displayed in Figure 6.16, where the *orthodiagonal*

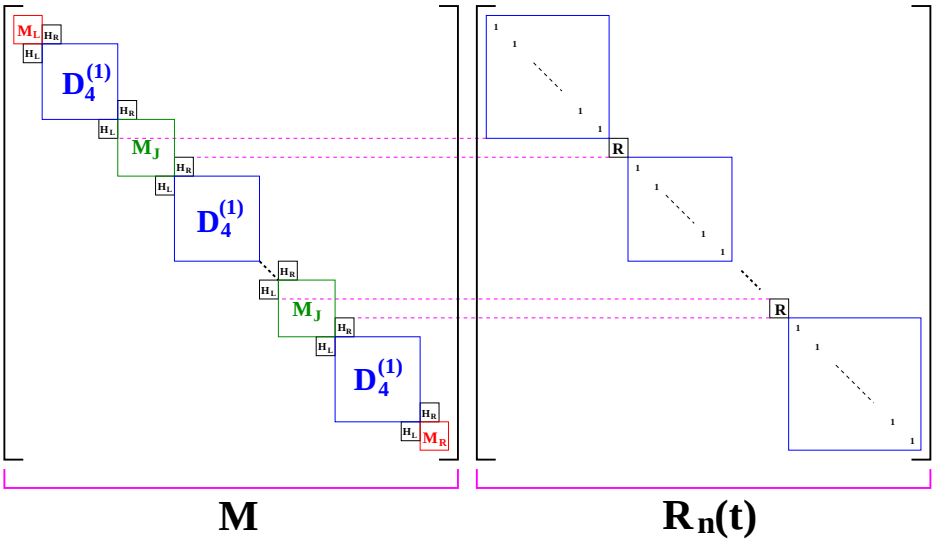

Figure 6.16: The Norm Matrix - 4^{th}-Order

blocks, H_L and H_R, are given by

$$H_L := \begin{pmatrix} -1 & 16 \\ 0 & -1 \end{pmatrix}, \quad H_R := \begin{pmatrix} -1 & 0 \\ 16 & -1 \end{pmatrix}. \tag{6.57}$$

For a $2\kappa \times 2\kappa$ M_J block, R is set as a $2(\kappa-2) \times 2(\kappa-2)$ block, thus setting $\kappa = 4$, and

$$R := \frac{1}{36} \begin{pmatrix} 37 & -4 & -4 & 1 \\ -4 & 52 & 16 & -4 \\ -4 & 16 & 52 & -4 \\ 1 & -4 & -4 & 37 \end{pmatrix} > 0 \quad , \quad R \in Mat_4^{Sym}, \tag{6.58}$$

assures the $\langle \boldsymbol{V}_J, R\boldsymbol{V}_J \rangle = \langle \overline{\boldsymbol{V}}_J, \overline{\boldsymbol{V}}_J \rangle$, where

$$\boldsymbol{V}_J := (v_{-2}, v_{-1}, v_1, v_2)^T, \quad \overline{\boldsymbol{V}}_J := \left(v_{-2}, v_{-1}, \frac{-v_{-2} + 4v_{-1} + 4v_1 - v_2}{6}, v_1, v_2 \right)^T. \tag{6.59}$$

Accordingly, by setting

$$M_J := \begin{pmatrix} -30 & 16 & -1 & & & & & \\ 16 & -30 & 16 & -1 & & & & \\ -\frac{69}{70} & \frac{556}{35} & -\frac{148}{5} & \frac{76}{5} & -\frac{4}{5} & \frac{2}{5} & -\frac{4}{35} & \frac{1}{70} \\ -\frac{2}{35} & \frac{2}{35} & \frac{54}{5} & -\frac{89}{5} & \frac{56}{5} & -\frac{26}{5} & \frac{37}{35} & -\frac{2}{35} \\ -\frac{2}{35} & \frac{37}{35} & -\frac{26}{5} & \frac{56}{5} & -\frac{89}{5} & \frac{54}{5} & \frac{2}{35} & -\frac{2}{35} \\ \frac{1}{70} & -\frac{4}{35} & \frac{2}{5} & -\frac{4}{5} & \frac{76}{5} & -\frac{148}{5} & \frac{556}{35} & -\frac{69}{70} \\ & & & & -1 & 16 & -30 & 16 \\ & & & & & -1 & 16 & -30 \end{pmatrix}, \tag{6.60}$$

we get that the minimal eigenvalue analysis of the matrix $-M^S$ remains identical to Case 1:

$$c_n \;:=\; -\max_{t_n \le t \le t_{n+1}} \left\{\sigma\left(M^S\right)\right\} \;\ge\; -\overline{\varepsilon}_m \max\left\{\sigma\left(\frac{1}{h^2} D_2^{(1)}\right)\right\} \;>\; \left(\frac{\pi}{5}\right)^2, \tag{6.61}$$

where $[R_n M]^S := \left([R_n M] + [R_n M]^T\right)/2$, $\overline{\varepsilon}_m$ is defined by

$$\overline{\varepsilon}_m \;:=\; \sup\left\{ \varepsilon \in (0,1) \,\middle|\, [R_n M]^S - \frac{1}{h^2}\left[\frac{\varepsilon D_4^{(1)} - (1-\varepsilon)\overline{\overline{D}}_4^{(0)}}{12}\right] \le 0 \right\} = \varepsilon_m \tag{6.62}$$

and the matrix $\overline{\overline{D}}_4^{(0)}$ is set by positioning $\left[\phi_3, D_4^{(0)}, \phi_4, D_4^{(0)}, \ldots \phi_4, D_4^{(0)}, \phi_3\right]$ blocks along the main diagonal, as displayed in Figure 6.17.

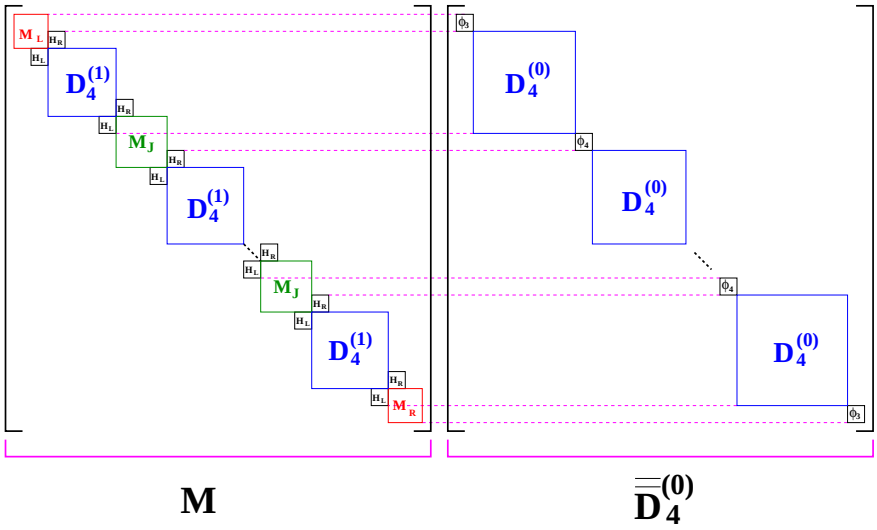

Figure 6.17: The $\overline{\overline{D}}_4^{(0)}$ Matrix - 4^{th}-Order

7 Numerical Examples

In this section two numerical examples are given: in 1-D and in 2-D. Note that, by the **CFL** condition, the temporal step satisfies $k = O(h^2)$, independently of the boundary's position.

7.1 One-Dimensional Example

Consider the one-dimensional diffusion equation with Dirichlet boundary condition,

$$\begin{aligned} \frac{\partial u}{\partial t} &= \frac{1}{4}\frac{\partial^2 u}{\partial x^2} + f(x,t) && (7.1)\\ u(\boldsymbol{x},0) &= sin(\pi/8), && (7.2)\\ u(\boldsymbol{x},t)\mid_{\partial\Omega(t)} &= u_B(t). && (7.3) \end{aligned}$$

We attempt to numerically solve it on a time dependent domain, $\Omega(t) \subset I_1 := [0,1]$, which is defined by,

$$\Omega(t) := \ \Omega_i(t) \quad if \quad \tfrac{i-1}{4} \le t \le \tfrac{i}{4} \qquad \forall\, t \in [0,1] \tag{7.4}$$

where:

$$\begin{aligned} \Omega_1(t) &:= \left(\frac{2-\sin(5\pi t)}{16}, \frac{5+48t^2}{16}\right) && (7.5)\\ &\quad \cup \left(\frac{8+e^{-4t}\sin(8\pi t)}{16}, \frac{7+\sqrt{t}}{8}\right), && (7.6)\\ \Omega_2(t) &:= \left(\frac{2-\sin(5\pi t)}{16}, \frac{16+e^{(t-1/4)/4}}{16}\right), && (7.7)\\ \Omega_3(t) &:= \left(\frac{2-\sin(5\pi t)}{16}, \frac{10-\sin(\pi(t-1/2))}{16}\right) && (7.8)\\ &\quad \cup \left(\frac{10+\sin(\pi(t-1/2))}{16}, \frac{16-e^{(t-1/4)/4}}{16}\right),\\ \Omega_4(t) &:= \left(\frac{2-\sin(5\pi t)}{16}, \frac{12-\sin(2\pi(t-3/4))}{32}\right)\\ &\quad \cup \left(\frac{3}{8}+\frac{\sin(8\pi(t-3/4))}{16/(5/4-t))}, \frac{10-\sin(\pi(t-1/2))}{16}\right)\\ &\quad \cup \left(\frac{10+\sin(\pi(t-1/2))}{16}, \frac{16-e^{(t-1/4)/4}}{16}\right), && (7.9) \end{aligned}$$

as displayed in Figure 7.1.

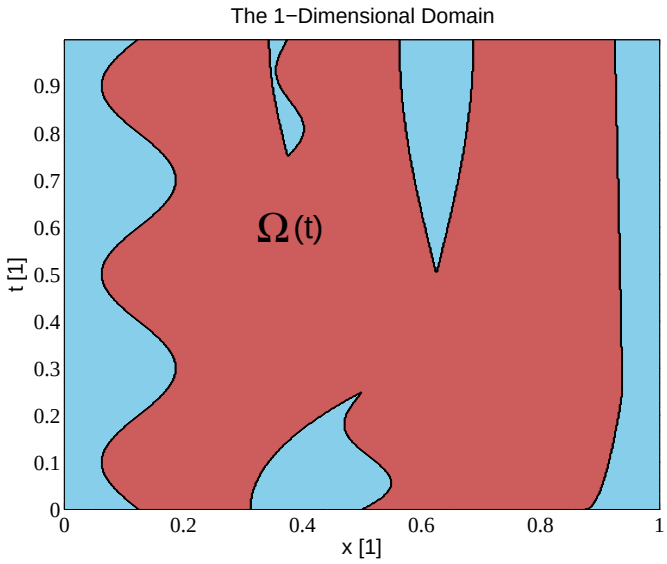

Figure 7.1: One-Dimensional Domain: Numerical Example

In order to have an exact error analysis, we set both the inhomogeneous term, $f(x,t)$, and the boundary values, $\{u_B(t)\}$, such that the exact solution is given by:

$$u \;=\; \sin\left(4\pi t x + \pi\left(t - \frac{1}{2}\right)^3\right) \tag{7.10}$$

We propagate the solution in time from $t = 0$ to $t = 1$ using mesh spacing h and corresponding time step $k = \frac{h^2}{4}$ for each of the following values:

$$h = \frac{1}{50}\ ,\ \frac{1}{75}\ ,\ \frac{1}{100}\ ,$$

where these values of h and the ratio $\frac{k}{h^2} = \frac{1}{4}$, can be shown to satisfy the bound requirement on the boundaries movement (3.2).

Since $k = O(h^2)$ it may be sufficient to use first order accurate time step scheme for the 2^{nd}-order spatial solution, and a second order time stepping scheme for the 4^{th}-order spatial solution. However, since our convergence analysis was done in semi-discrete settings, we take extra precaution and use **RK2** and **RK4** for the 2^{nd}-order and 4^{th}-order spatial approximations

respectively. For each run (with a different h value from $t = 0$ to $t = 1$), we compute the exact local error at each time step, which is simply the difference between the computed solution and the exact solution at every grid point. We analyze the results by displaying them on two graphs in the standard form of $\ln \|error\|$ vs. $\ln |1/h|$:

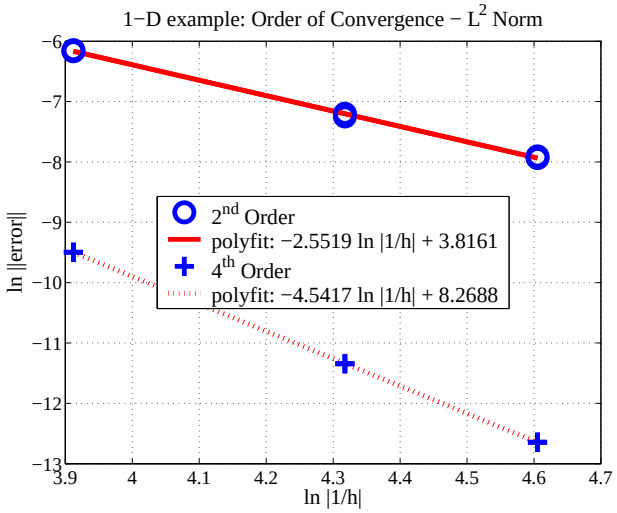

Figure 7.2: One-Dimensional Numerical Result - L^2 Norm at $t = 1$

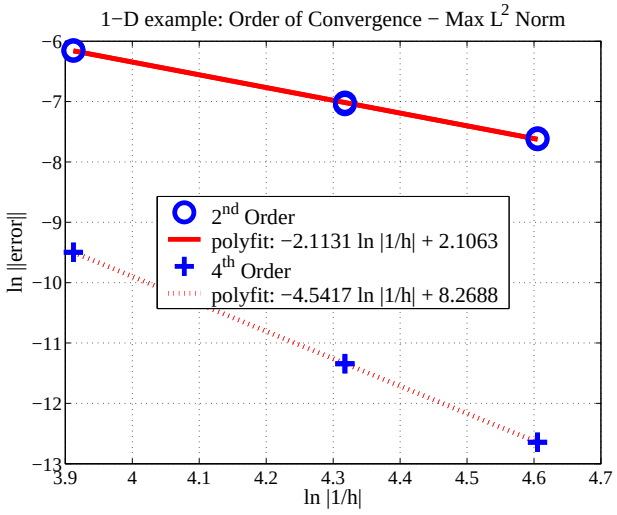

Figure 7.3: One-Dimensional Numerical Result - Max L^2 Norm over time

In figure 7.2, the norm $\|\cdot\|$, is $\|\cdot\|_n$ (as defined in 4.1) for each mesh size h at $t = 1$, and in figure 7.3, the norm $\|\cdot\|$, is taken as the $\max_{0\leq\nu\leq n}\|\cdot\|_\nu$ norm for each mesh size h, and for $0 \leq t \leq 1$.

The poly-fitted slopes of the error graphs indicate that the method is indeed 2^{nd}-order and 4^{th}-order convergent, with respect to the accuracy order of the spatial approximation.
Note, that in both figures the poly-fitted error graph of the 4^{th}-order spatial solution is identical, this result is due to the fact that for this particular example we got the maximal error at the final time point, $t = 1$.

7.2 Two-Dimensional Example

In this example, we consider the two-dimensional diffusion equation with Dirichlet boundary condition,

$$\frac{\partial u}{\partial t} = \frac{1}{4}\left[\frac{\partial^2 u}{\partial x^2} + \frac{\partial^2 u}{\partial y^2}\right] + f(x, y, t) \tag{7.11}$$

$$u(\boldsymbol{x}, 0) = 0, \tag{7.12}$$

$$u(\boldsymbol{x}, t)\mid_{\partial\Omega(t)} = u_B(t). \tag{7.13}$$

on the following two-dimensional domain:

$$\Omega(t) := \Omega_s(t) \cap \Omega_m(t) \subset I_2 := [0, 1] \times [0, 1], \tag{7.14}$$

where:

$$\Omega_s(t) := \left\{(x, y) \in \mathbb{R}^2 \,\middle|\, \left(x - \frac{1}{2}\right)^2 + \left(y - \frac{1}{2}\right)^2 < \left(\frac{5}{12}\right)^2\right\}, \tag{7.15}$$

$$\Omega_m(t) := \left\{(x, y) \in \mathbb{R}^2 \,\middle|\, \left(x - \left(\frac{1}{2} + \frac{1}{6}\cos(2\pi t - \pi)\right)\right)^2 \right. \tag{7.16}$$

$$\left. + \left(y - \left(\frac{1}{2} + \frac{1}{6}\sin(2\pi t)\right)\right)^2 > \left(\frac{1}{12}\right)^2\right\}, \tag{7.17}$$

as described graphically in Figure 7.4.
As in the one-dimensional example, we set the inhomogeneous term, $f(x, t)$, and the boundary values, $\{u_B(t)\}$, such that the exact solution is given by:

$$u = \sin(t)\cos\left(2\pi(x^2 + y^2)\right) \tag{7.18}$$

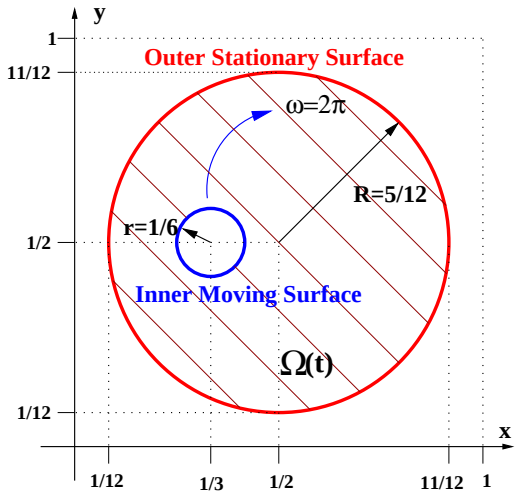

Figure 7.4: Two-Dimensional Domain: Numerical Example

We propagate the solution in time from $t = 0$ to $t = 1$ using mesh spacing h and time step $k = \frac{h^2}{4}$ for the same values of h as in the previous example. These settings can be shown to satisfy both the bound requirement on the boundaries movement (3.2) for every one-dimensional section of the domain, and the relevant multi-dimensional requirements (i.e. the Intersection and Curvature Conditions as described in section 3.2.1).

We apply the scheme with **RK2** for the 2^{nd}-order spatial approximation, and **RK4** for the 4^{th}-order spatial approximation. The results are displayed in the same manner as in the previous example in Figures 7.5 and 7.6.

As in the previous example, the poly-fitted slopes of the error graphs indicate that the method is indeed 2^{nd}-order and 4^{th}-order convergent, with respect to the accuracy order of the spatial approximation.

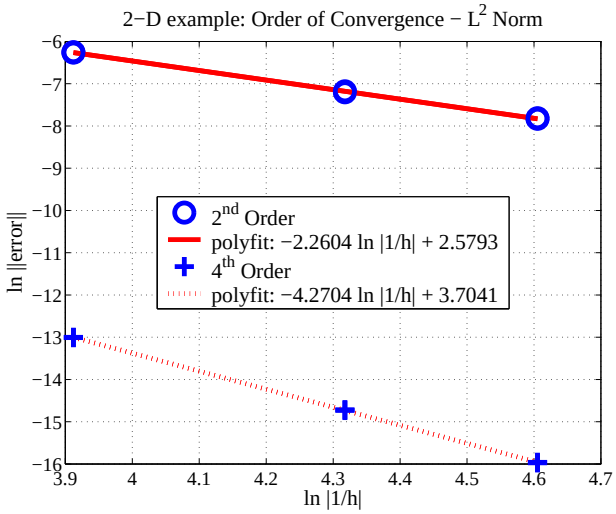

Figure 7.5: 2-D Numerical Result - L^2 Norm at $t = 1$

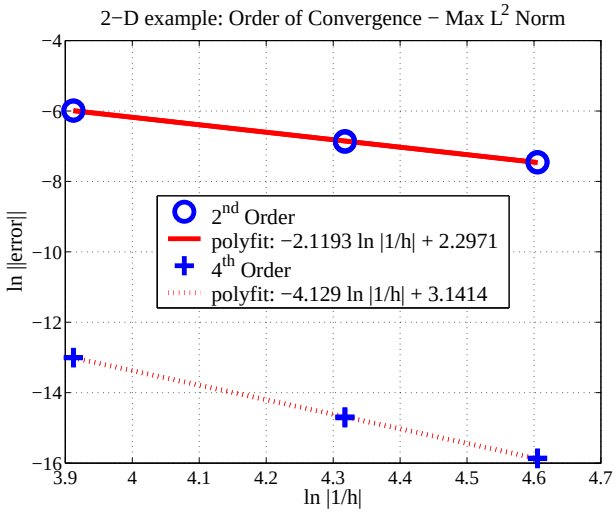

Figure 7.6: 2-D Numerical Result - Max L^2 Norm over time

8 Conclusions

In this work we have addressed the problem of finding numerical solutions to parabolic and hyperbolic equations on irregular multi-dimensional domains with time evolving impenetrable boundaries. We performed a comprehensive theoretical study of the numerical issues, that arise when dealing with time

dependent domains. Compared to other works, which deal with Embedded Methods for moving boundary problems, this work contains some significant contributions:

- Applies to very complex moving geometries, including mergers and breakups of the moving boundaries.
- Contains a through convergence analysis, which applies to multi-dimensional geometries of any finite dimension.
- Can be implemented with high orders of, both temporal and spatial accuracies, as has been demonstrated in this article.
- The resulting method is strictly stable, which implies that the solution remains consistent and valid for long integration time.

Two major difficulties had to be dealt with. The first, was a result of the multi-dimensional boundary movement. It was shown that no matter how small the boundary may move in the normal direction, very large variations of boundary points can occur at some one-dimensional section of the domain. The second, became apparent when we attempted to implement the theoretical study for the diffusion equation - events of mergers and breakups of the moving boundaries, led to Indefiniteness of the numerical operator in the standard euclidian inner product. This phenomena is fundamentally problematic, because the Negative Definiteness property of the numerical operator was required for both the strict stability analysis, and the applicability of the method to multi-dimensional domains.
These difficulties were tackled by:

- Introducing a new inner product for the genuine one-dimensional case.
- Inserting entering grid-points as they become admissible within the multi-stage solution method, for the multi-dimensional case.

The numerical examples, indeed, demonstrated the efficiency of the method for multi-dimensional high-order of accurate solutions. For future study there are, still, several unresolved issues, which are, among others:

- Introduction of a proper inner product, which allows preservation of the Negative-Definiteness of the numerical operator, without reinsertion of grid-points in the multi-dimensional case.
- Extension of the method to allow treatment of other boundary conditions, as well as moving interface problems, such as the Stefan problem.

A The Fundamental Matrices

In this appendix we analyze the matrices resulting from the application of the algorithm with the diffusion equation. The main concerns are N.D (N.P.D) analysis of the matrices, and the approximation of the maximal eigenvalue.

A.1 The 2nd-Order Numerical Diffusion Operator

The general structure we wish to explore is given by the $N_0 \times N_0$ matrix:

$$D_2(a) := \begin{pmatrix} a & 1 & & & \\ 1 & -2 & 1 & & \\ & \ddots & \ddots & \ddots & \\ & & 1 & -2 & 1 \\ & & & 1 & a \end{pmatrix}, \quad a \in \mathbb{R}. \tag{A.1}$$

A.1.1 Analysis of $D_2^{(1)}$

The first observation is that $D_2^{(1)} = D_2(-2)$ is indeed N.D., since it satisfies

$$D_2^{(1)} \leq -U_2^T U_2 < 0, \tag{A.2}$$

where U_2 is an $N_0 \times N_0$ non-singular matrix:

$$U_2 := \begin{pmatrix} 1 & -1 & & & \\ & 1 & -1 & & \\ & & \ddots & \ddots & \\ & & & 1 & -1 \\ & & & & 1 \end{pmatrix}, \quad -U_2^T U_2 = \begin{pmatrix} -1 & 1 & & & \\ 1 & -2 & 1 & & \\ & \ddots & \ddots & \ddots & \\ & & 1 & -2 & 1 \\ & & & 1 & -2 \end{pmatrix}. \tag{A.3}$$

Indeed, for $N_0 \gg 1$, we have

$$\max\left[\sigma\left(D_2^{(1)}\right)\right] = -\frac{\pi^2}{(N_0+1)^2} + O\left(\frac{1}{N_0^4}\right), \tag{A.4}$$

see [25] for details.

A.1.2 Analysis of $D_2^{(0)}$

The matrix $D_2^{(0)}$ is the matrix satisfying

$$D_2^{(0)} = D_2(a_0) \quad : \quad D_2^{(0)} \text{ is N.P.D}, \tag{A.5}$$

for some $a_0 > -2$. We denote by $D_{2,L}(a_0)$ the upper-left $(N_0-1)\times(N_0-1)$ block of $D_2(a_0)$ as displayed in Figure A.1.

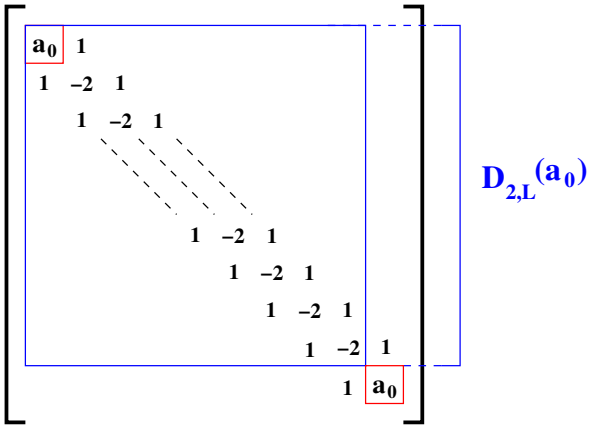

Figure A.1: The Upper-Left Block - 2nd-Order

Assuming $D_{2,L}(a_0) < 0$, we may apply a congruence transformation,

$$C^T \overline{D}_2(a_0) C \;=\; D_2(a_0), \tag{A.6}$$

with a non-singular matrix C, which is constructed as displayed in Figure A.2,

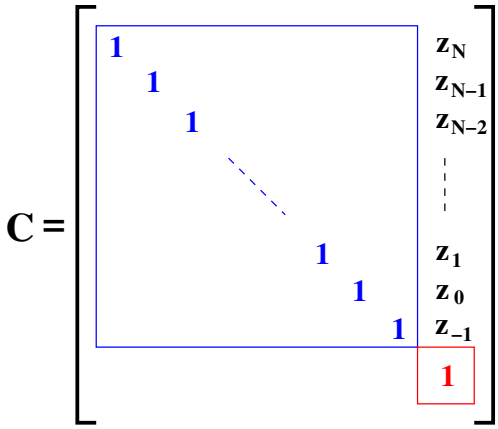

Figure A.2: The Fundamental Congruence Matrix - 2nd-Order

where $N := N_0 - 3$, and the elements $\{z_j\}_{j=-1}^{N}$ are uniquely determined by

the difference equation,

$$z_j = 2z_{j-1} - z_{j-2}\ ,\ j \in \{1, 2, \dots N\}, \tag{A.7}$$

with an initial and a terminal conditions

$$z_0 - 2z_{-1} = 1, \tag{A.8}$$

$$a_0 \cdot z_N + z_{N-1} = 0. \tag{A.9}$$

This yields a congruent matrix, $\overline{D}_2(a_0)$, as displayed in Figure A.3,

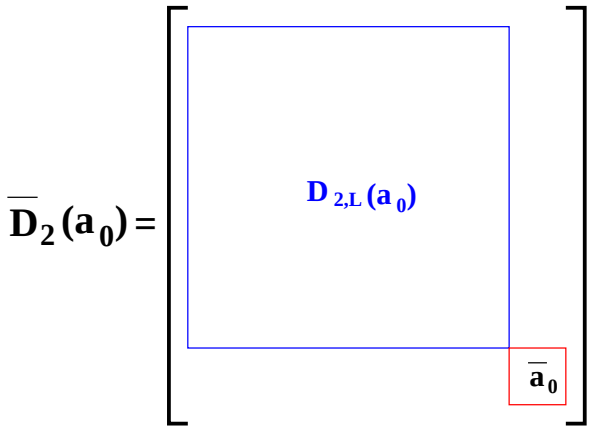

Figure A.3: The Equivalent Matrix $\overline{D}_2(a_0)$

whose 1×1 lower-right corner is given by

$$\overline{a}_0 \ = \ a_0 + \delta_0, \quad \delta_0 \ := \ -z_{-1} \ = \ \frac{(a_0+1)(N_0+1)-1}{(a_0+1)(N_0+2)-1}. \tag{A.10}$$

Indeed, it is easily seen that, for any N_0 sufficiently large,

$$\begin{cases} -1 < a_0 < -2 & \longrightarrow \quad \overline{a}_0 < 0 \\ a_0 = -1 & \longrightarrow \quad \overline{a}_0 = 0 \end{cases}, \tag{A.11}$$

hence,

$$D_2^{(0)} \ = \ D_2(a_0 = -1). \tag{A.12}$$

Note that, by the analysis for $D_2^{(1)}$, we have $a_0 = -1 \quad \Rightarrow \quad D_{2,L}(a_0) < 0$, thus by (A.3) the congruence transformation is justified, and the elements $\{z_j\}_{j=-1}^{N}$ are uniquely determined.

A.2 4^{th}-Order Numerical Diffusion Operator

The general structure we wish to explore is given by the $N_0 \times N_0$ matrix:

$$D_4(a,b,c) := \begin{pmatrix} a & b & -1 & & & & \\ b & c & 16 & -1 & & & \\ -1 & 16 & -30 & 16 & -1 & & \\ & \ddots & \ddots & \ddots & \ddots & \ddots & \\ & & -1 & 16 & -30 & 16 & -1 \\ & & & -1 & 16 & c & b \\ & & & & -1 & b & a \end{pmatrix}. \tag{A.13}$$

A.2.1 Analysis of $D_4^{(1)}$

The first observation is that $D_4^{(1)} = D_4(-30, 16, -30)$ is indeed N.D, since it satisfies,

$$D_4^{(1)} \leq -U_4^T U_4 < 0, \tag{A.14}$$

where U_4 is an $N_0 \times N_0$ non-singular matrix, given by

$$U_4 := \begin{pmatrix} 2-\sqrt{3} & -4 & 2+\sqrt{3} & & & & & \\ & 2-\sqrt{3} & -4 & 2+\sqrt{3} & & & & \\ & & 2-\sqrt{3} & -4 & 2+\sqrt{3} & & & \\ & & & \ddots & \ddots & \ddots & & \\ & & & & 2-\sqrt{3} & -4 & 2+\sqrt{3} & \\ & & & & & 2-\sqrt{3} & -4 & \\ & & & & & & 2-\sqrt{3} & \end{pmatrix}, \tag{A.15}$$

whose $-U_4^T U_4$ multiplication satisfies the equality given in Figure A.4,

$$-\mathbf{U_4^T U_4} = \begin{bmatrix} \underline{-\mathbf{H}} & -1 & & & & & \\ 16 & -1 & & & & & \\ -1 & 16 & -30 & 16 & -1 & & \\ & -1 & 16 & -30 & 16 & -1 & \\ & & \ddots & \ddots & \ddots & \ddots & \ddots \\ & & & -1 & 16 & -30 & 16 & -1 \\ & & & & -1 & 16 & -30 & 16 \\ & & & & & -1 & 16 & -30 \end{bmatrix} < \mathbf{0}$$

Figure A.4: The Matrix $-U_4^T U_4$

where the block $\underline{H}$ is given by,

$$\underline{H} := \begin{pmatrix} 7-4\sqrt{3} & -8+4\sqrt{3} \\ -8+4\sqrt{3} & 23-4\sqrt{3} \end{pmatrix} > 0. \tag{A.16}$$

We have $D_4^{(1)} = 12D_2^{(1)} - \left(D_2^{(1)}\right)^2 + E$, where

$$E := \begin{pmatrix} -1 & & & & \\ & 0 & & & \\ & & \ddots & & \\ & & & 0 & \\ & & & & -1 \end{pmatrix} \leq 0, \tag{A.17}$$

hence, $D_4^{(1)} < 12D_2^{(1)}$, and consequently using section (A.1.1) we get

$$\max\left[\sigma\left(D_4^{(1)}\right)\right] < 12\max\sigma\left(D_2^{(1)}\right) \approx -12\frac{\pi^2}{(N_0+1)^2}. \tag{A.18}$$

A.2.2 Analysis of $D_4^{(0)}$

The matrix $D_4^{(0)}$ is the matrix satisfying

$$D_4^{(0)} = D_4(a_0, b_0, c_0) \quad : \quad D_4^{(0)} \text{ is N.P.D}, \tag{A.19}$$

for some $a_0, b_0, c_0 \in \mathbb{R}$. We denote by $D_{4,L}(a_0, b_0, c_0)$, the $(N_0-2)\times(N_0-2)$ upper-left block of $D_4(a_0, b_0, c_0)$ as displayed in Figure A.5.

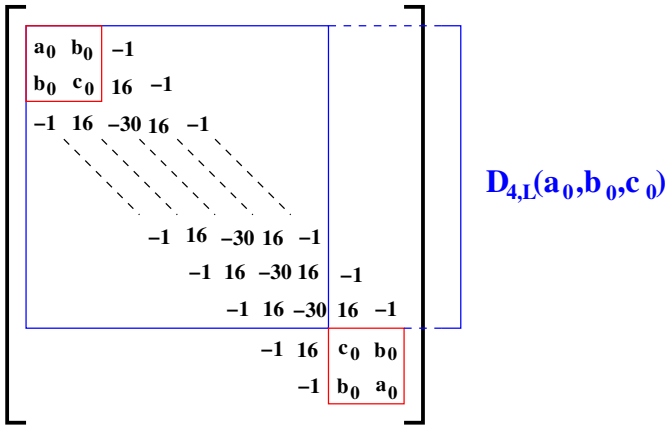

Figure A.5: The Upper-Left Block - 4$^{\text{th}}$-Order

Assuming $D_{4,L}(a_0, b_0, c_0) < 0$, we may apply a congruence transformation,

$$C^T \overline{D}_4(a_0, b_0, c_0) C \;=\; D_4(a_0, b_0, c_0), \tag{A.20}$$

using a non-singular matrix C, which is constructed as displayed in Figure A.6,

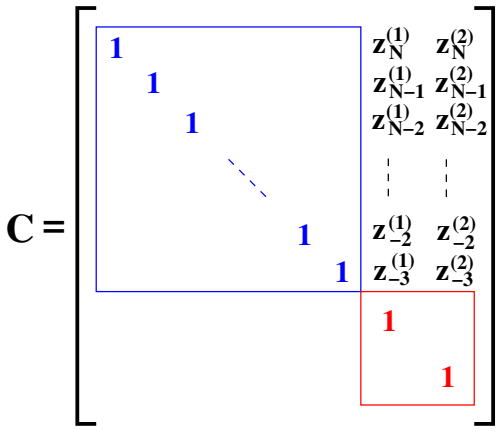

Figure A.6: The Fundamental Congruence Matrix - 4^{th}-Order

where $N := N_0 - 6$. The elements $\left\{z_j^{(i)}\right\}_{j=-3}^{N}$ are uniquely determined by the difference equation,

$$z_j^{(i)} \;=\; 16z_{j-1}^{(i)} - 30z_{j-2}^{(i)} + 16z_{j-3}^{(i)} - z_{j-4}^{(i)}, \quad i = 1, 2, \quad j \in \{1, 2, \ldots N\}, \tag{A.21}$$

with the initial conditions:

$$-z_{-1}^{(i)} + 16z_{-2}^{(i)} - 30z_{-3}^{(i)} \;=\; \begin{cases} 16 & \text{if } i = 1 \\ -1 & \text{if } i = 2 \end{cases}, \tag{A.22}$$

$$-z_{0}^{(i)} + 16z_{-1}^{(i)} - 30z_{-2}^{(i)} + 16z_{-3}^{(i)} \;=\; \begin{cases} -1 & \text{if } i = 1 \\ 0 & \text{if } i = 2 \end{cases}, \tag{A.23}$$

and the terminal conditions:

$$a_0 z_N^{(i)} + b_0 z_{N-1}^{(i)} - z_{N-2}^{(i)} \;=\; 0, \tag{A.24}$$

$$b_0 z_N^{(i)} + c_0 z_{N-1}^{(i)} + 16z_{N-2}^{(i)} - z_{N-3}^{(i)} \;=\; 0. \tag{A.25}$$

This yields an equivalent matrix, $\overline{D}_4(a_0, b_0, c_0)$, as displayed in Figure A.7,

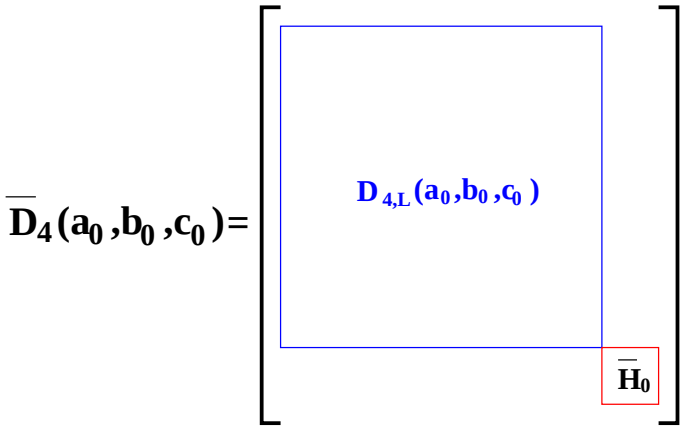

Figure A.7: The Equivalent Matrix $\overline{D}_4(a_0, b_0, c_0)$

whose 2×2 lower-right corner, $\overline{H}_0$, is given by

$$\overline{H}_0 \;=\; \begin{pmatrix} c_0 & b_0 \\ b_0 & a_0 \end{pmatrix} + \Delta_0, \quad \Delta_0 \;:=\; \begin{pmatrix} -16z_{-3}^{(1)} + z_{-2}^{(1)} & z_{-3}^{(1)} \\ z_{-3}^{(1)} & z_{-3}^{(2)} \end{pmatrix}. \tag{A.26}$$

Accordingly, by denoting

$$-H_0 \;:=\; \begin{pmatrix} a_0 & b_0 \\ b_0 & c_0 \end{pmatrix} \;\leq\; -\underline{H}, \tag{A.27}$$

it can be shown that

$$H_0 = -\underline{H} \;\Longrightarrow\; \Delta_0 = \overline{H}^R, \tag{A.28}$$

$$H_0 = -\overline{H} \;\Longrightarrow\; \Delta_0 = \underline{H}^R, \tag{A.29}$$

where $\underline{H}$ is as given in (A.16), and $\overline{H}$ is given by

$$\overline{H} \;:=\; \begin{pmatrix} 7+4\sqrt{3} & -8-4\sqrt{3} \\ -8-4\sqrt{3} & 23+4\sqrt{3} \end{pmatrix} \;\geq\; \underline{H} \;>\; 0. \tag{A.30}$$

The symbol $[\quad]^R$ denotes a reflection operator at the secondary diagonal

$$H^R := \begin{pmatrix} c_1 & b_1 \\ b_1 & a_1 \end{pmatrix} \quad \forall\, H = \begin{pmatrix} a_1 & b_1 \\ b_1 & c_1 \end{pmatrix} \in\; Mat_2^{Sym}. \tag{A.31}$$

Indeed, by setting:

$$H_0 \;=\; -\varepsilon\overline{H} - (1-\varepsilon)\underline{H} \;<\; 0 \quad \forall\, \varepsilon \in [0,1], \tag{A.32}$$

it can be shown that

$$\Delta_0 \;=\; \frac{\varepsilon \underline{H}^R \cdot \lambda_1^{N+4} + (1-\varepsilon)\overline{H}^R \cdot \lambda_2^{N+4}}{\varepsilon \cdot \lambda_1^{N+4} + (1-\varepsilon)\cdot \lambda_2^{N+4}}, \quad \lambda_{1,2} \;:=\; 7 \pm 4\sqrt{3}, \tag{A.33}$$

and in particular we have

$$\begin{cases} 0 \le \varepsilon < \varepsilon_0 & \longrightarrow & \overline{H}_0 \ge 0 \\ \varepsilon = \varepsilon_0 & \longrightarrow & \overline{H}_0 = 0\,, \\ \varepsilon_0 < \varepsilon \le 1 & \longrightarrow & \overline{H}_0 \le 0 \end{cases} \qquad \varepsilon_0 := \frac{1}{1+\lambda_1^{N+4}}, \tag{A.34}$$

hence,

$$D_4^{(0)} \;=\; D_4(a_0, b_0, c_0)|_{H_0 = -\varepsilon_0 \overline{H} - (1-\varepsilon_0)\underline{H}}\,. \tag{A.35}$$

Note that,

$$-\varepsilon_0 \overline{H} - (1-\varepsilon_0)\underline{H} \;=\; -\underline{H} - \frac{8\sqrt{3}}{\left(7+4\sqrt{3}\right)^{N_0-2}} \begin{pmatrix} 1 & -1 \\ -1 & 1 \end{pmatrix} \tag{A.36}$$

$$\le\; -\underline{H}, \tag{A.37}$$

hence, by the analysis for $D_4^{(1)}$, we have

$$H_0 \le -\underline{H} \quad \Rightarrow \quad D_{4,L}(a_0, b_0, c_0) \;<\; 0, \tag{A.38}$$

which assures that the congruence transformation is justified, and the elements $\left\{z_j^{(i)}\right\}_{j=-3}^{N}$ are uniquely determined.

References

[1] J. Crank, Free and Moving Boundary Problems. Oxford University Press, Inc., 1987.

[2] C. A. Brebbia, B. Šarler (Editors), Moving Boundaries VI: Computational Modelling of Free and Moving Boundary Problems. WIT Press, Inc., 2001.

[3] C. A. Brebbia, A. A. Mammoli (Editors), Moving Boundaries VII: Computational Modelling of Free and Moving Boundary Problems (Computational and Experimental Problems). WIT Press, Inc., 2003.

[4] Y. Harness, Embedded Finite-Difference Schemes for Initial Boundary Value Problems in Time Dependent Complex Domains. *Thesis submitted for the degree "Master of Science"*, **Tel-Aviv University**. 2006.

[5] C. S. Peskin, Numerical analysis of blood flow in the heart. *J. Comp. Phys.*, **25**, pp. 220-252. 1997.

[6] C. S. Peskin, The immersed boundary method. *Acta Numer.*, **11**, pp. 479-517. 2002.

[7] R.P. Fedkiw, T. Aslam, B. Merriman and S. Osher, A non-oscillatory Eulerian approach to interface in multimaterial flows (the Ghost Fluid Method). *J. Comput. Phys.*, **152**, pp. 457-492, 1999.

[8] M. Kang, R.P. Fedkiw and X.-D. Liu, A boundary condition capturing method for multiphase incompressible flow. *Sci. Comput.*, **15**, pp. 323-360, 2000.

[9] F. Gibou and R. Fedkiw, A fourth order accurate discretization for the Laplace and heat equations on arbitrary domain with applications to the Stefan problem. *J. Comput. Phys.*, **202**, pp. 577-601, 2005.

[10] A. Mayo, The fast solution of Poisson's and biharmonic equations on irregular regions. *SIAM J. Numer. Anal.*, **21**(?), pp. 285-299, 1984.

[11] R.J. LeVeque and Z. Li, The immersed interface method for elliptic equations with discontinuous coefficients and singular sources. *SIAM J. Numer. Anal.*, **31**, pp. 1001-1025, 1994.

[12] Z. Li, K. Ito, The Immersed Interface Method: Numerical Solutions of PDEs Involving Interfaces and Irregular Domains. *SIAM (Frontiers in Applied Mathematics)*, July 2006.

[13] T. Y. Hou, Z. Li, S. Osher, H. Zaho, A Hybrid method for Moving Interface Problems with Application to the Hele-Shaw Flow. *J. Comput. Phys.*, **134**, pp. 236-252, 1997.

[14] J. A. Sethian, Level Set Methods and Fast Marching Methods. Cambridge University Press, Inc., 1999.

[15] S. J. Osher, R. P. Fedwik, Level Set Methods and Dynamic Implicit Surfaces. Springer, Inc., 2002.

[16] H.S. Udaykumar, W. Shyy and M.M. Rao, Elafint: a mixed Eulerian-Lagrangian method for fluid flows with complex and moving boundaries. *Int. J. Numer. Methods in Fluids*, **22**(?), pp. 691-705, 1996.

[17] A.N. Almgren, J.B. Bell, P. Colella and T. Marthaler, A Cartesian grid projection method for the incompressible Euler equations in complex geometries. *SIAM J. Sci. Comput.*, **18**, pp. 1289-1309, 1997.

[18] H.S. Udaykumar, R. Mittal and W. Shyy, Computation of solid-liquid phase fronts in the sharp interface limit on fixed grids. *J. Comput. Phys.*, **153**, pp. 534-574. 1999.

[19] H.S. Udaykumar, R. Mittal, P. Rampunggoon and A. Khanna, A sharp interface Cartesian grid method for simulating flows with complex moving boundaries. *J. Comput. Phys.*, **174**, pp. 345-380, 2001.

[20] D. Russell and Z.J. Wang, A Cartesian grid method for modeling multiple moving objects in 2D incompressible viscous flow. *J. Comput. Phys.*, **191**, pp. 177-205, 2003.

[21] P. McCorquodale, P. Colella and H. Johansen, A Cartesian grid embedded boundary method for the heat equation on irregular domains. *J. Comput. Phys.*, **173**, pp. 620-635, 2001.

[22] P. Schwartz, M. Barad, P. Colella, T. Ligocki, A Cartesian Grid Embedded Boundary Method for the Heat Equation and Poisson's Equation in three dimensions. *J. Comput. Phys.*, **211**, pp. 531-550, 2006.

[23] M.H. Carpenter, D.Gottlieb and S. Abarbanel, Time Stable Boundary Conditions for Finite Difference Schemes Solving Hyperbolic Systems: Methodology and Application to High Order Compact Schemes. NASA Contractor Report 191436, ICASE Report 93-9, and *J. Comput. Phys.*, **111**(2), 1994.

[24] S. Abarbanel, A. Ditkowski, Multi-Dimensional Asymptotically Stable 4^{th}-Order Accurate Schemes for the Diffusion Equation. ICASE Report No.96-8, February 1996. Also, Asymptotically Stable Fourth-Order Accurate Schemes for the Diffusion Equation on Complex Shapes. *J. Comput. Phys.*, **133**(2), 1997.

[25] A. Ditkowski, Bounded-Error Finite Difference Schemes for Initial Boundary Value Problems on Complex Domains. *Thesis submitted for the degree "Doctor of Philosophy"*, **Tel-Aviv University**. 1997.

[26] S. Abarbanel, A. Ditkowski, Multi-dimensional asymptotically stable schemes for advection-diffusion equations. *Computers and Fluids*, **28**, 1999. 481-510. (also ICASE report 47-96).

[27] A. Ditkowski, K.H. Dridi, J.S. Hesthaven, Convergent Cartesian grid methods for Maxwell's equations in complex geometries. *J. Comput. Phys.*, **170**, 39-80. 2001.

[28] A. Ditkowski, K.H. Dridi, J.S. Hesthaven, Staircase-free finite-difference time-domain formulation for general materials in complex geometries. *IEEE Trans. Antennas Propagat.*, **AP-49**(5), 749–756, 2001.

[29] S. Abarbanel, A. Ditkowski, A. Yefet, Bounded-error schemes for the wave equation on complex domains. *Journal of Scientific Computing*, **26**(1), 67-81. 2006.

[30] H.O. Kreiss, L. Wu. On the Stability definition of Difference Approximations for the Initial Boundary Value Problems. *Appl. Num. Math.*, **12**, 1993, 213-227.

[31] D. Levy, E. Tadmor. From Semi-Discrete to Fully-Discrete: The Stability of Runge-Kutta Schemes by the Energy Method. *SIAM Review*, **40**(1), 40-73, 1998.

[32] B. Gustafsson. The convergence rate for difference approximations to mixed initial boundary value problems. *Math. Comp.* **29**, 296-406. 1975.

[33] B. Gustafsson. The convergence rate for difference approximations to general mixed initial boundary value problems. *SIAM J. Numer. Anal.* **18**(2), 179-190. 1981.

[34] S. Abarbanel, A. Ditkowski, B. Gustafsson. On error bounds of finite difference approximations to partial differential equations - temporal behavior and rate of convergence. *J. Comput. Phys.*, **170**, 79–116. 2000.